Pergamon

*Journal of Structural Geology*, Vol. 16, No. 12, pp. 1655 to 1674, 1994

0191-8141/94 $7.00 + 0.00

0191-8141(94)E0023-R

# Strain accommodation about strike-slip fault discontinuities in granitic rock under brittle-to-ductile conditions

ROLAND BÜRGMANN and DAVID D. POLLARD

Department of Geological and Environmental Sciences, Stanford University, Stanford, CA 94305-2115, U.S.A.

(*Received* 5 *March* 1993; *accepted in revised form* 10 *January* 1994)

**Abstract**—Brittle and ductile structures adjacent to fault terminations and echelon fault steps of left-lateral strike-slip faults in the Lake Edison Granodiorite of the central Sierra Nevada, California are related to stress perturbations caused by fault slip. The structures associated with fault terminations change from dilatant splay fractures only, to splay fractures and ductile fabrics on opposing sides of the fault, to ductile fabrics ahead of the fault with decreasing distance from a younger neighboring pluton and, presumably, with increased temperatures. The distributions of deformation mechanisms correlate with the inferred local magnitudes and spatial distributions of the maximum tensile stress, the mean stress, and the maximum shear stress. Displacements along the faults are transferred across echelon stepovers by mineralized dilatant fractures in extensional steps. To accommodate slip transfer across contractional steps, rock apparently was squeezed vertically out of the step by ductile flow; concentrations of mobile and immobile elements indicate that diffusive mass transfer was not significant. Increased mean stress in contractional steps apparently enhanced crystal-plastic flow of quartz. A flow law that includes a pressure effect through correlation with pressure-dependent solidus temperatures is more successful than other experimentally derived flow laws in predicting the observed distribution of ductile fabrics.

## INTRODUCTION

DISCONTINUITIES (steps, bends or breaks) along crustal strike-slip faults are potential initiation and arrest zones of earthquake ruptures (King & Nabelek 1985, Sibson 1986b, Harris & Day 1993). Earthquakes commonly initiate at the base of the seismically active fault zones where conditions are thought to be close to the brittle–ductile transition of crustal rocks (Sibson 1984). Therefore the study of fault stepovers that were active at transition conditions may offer insight into the initiation of fault ruptures and the mechanics of slip transfer across discontinuities.

First, we describe fault terminations and fault stepovers in granitic rock in the central Sierra Nevada, California (Fig. 1), that formed under conditions close to the brittle–ductile transition (Segall & Simpson 1986, Bürgmann & Pollard 1992). Next, we evaluate the effects of the stress field at fault terminations on the constitutive behavior of granitic rock at varying temperatures. Finally, we compare the field observations of fault steps with the stress field predicted by mechanical

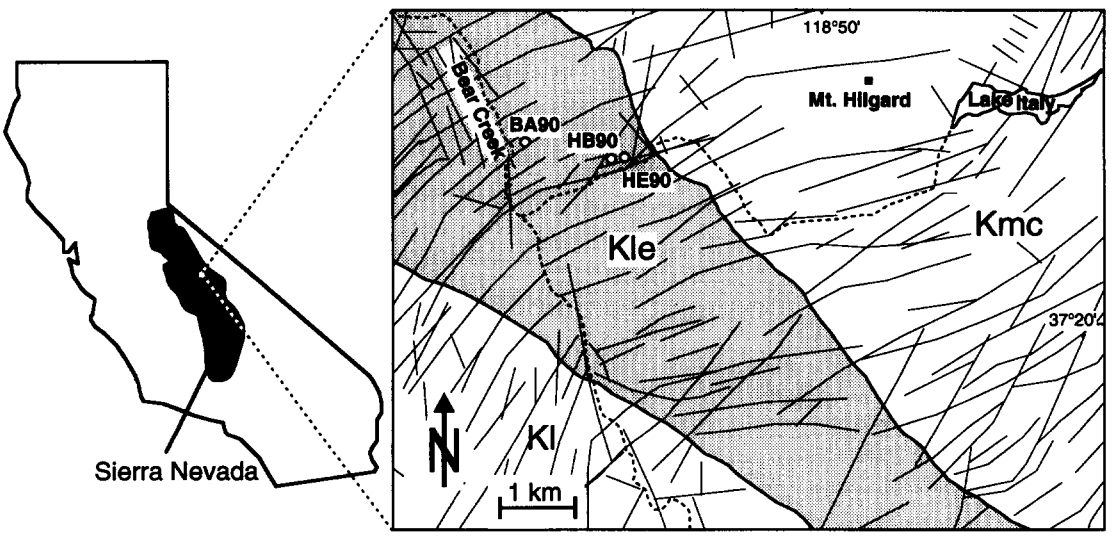


Fig. 1. Map showing Bear Creek region of Mt. Abbot quadrangle and the location of the numbered outcrops described in this paper. Pluton contacts are shown in heavy lines and major stream valleys are dashed. Kl—Lamarck Granodiorite, Kle—Lake Edison Granodiorite, Kmc—Mono Creek Granite. The plutons intruded sequentially from west to east in the Late Cretaceous. Thin lines are photo lineaments marked by vegetation and small channels that apparently follow strike-slip fault zones that developed along previously formed joints in the area.

models. Our analysis suggests that deformation laws for granitic rock should include a pressure weakening effect (Bürgmann & Pollard 1992). The Sierran faults described in this paper can be considered natural experiments that give us further insight into the mechanics of rock deformation at hydrothermal conditions and geological deformation rates.

*Deformation along discontinuous faults*

Deformation along faults is concentrated at their *peripheries* and around discontinuities over a wide range of length scales and geologic settings (Chinnery 1965, Rodgers 1980, Segall & Pollard 1980, Aydin & Nur 1982). Where faults terminate or deviate from their trace, strain from fault slip must be distributed in the surrounding rock by elastic straining, fracture, and/or flow. The characteristics of the deformation change with scale, depend on material properties and pressure–temperature conditions, and are influenced by heterogeneity in the wall rock, the seismic or aseismic nature of faulting, and the cumulative slip magnitude on the adjoining fault segments.

At the lateral strike-slip fault peripheries (mode II crack tips, Lawn & Wilshaw 1975, p. 51), dilatant *splay fractures*, normal faults, or other extensional structures may propagate away from the *fault termination* following the orientation of the local maximum principal compressive stress (Brace & Bombolakis 1963, Tapponnier & Brace 1976, Wong 1982, Granier 1985, Deng *et al.* 1986). Contractional structures such as pressure solution seams (Fletcher & Pollard 1981), folds and thrust faults (Deng *et al.* 1986) may form on the opposite side of the fault termination and trend parallel to the local minimum principal stress. At the crustal scale, subsidence in the extensional quadrants and uplift in the antisymmetric contractional quadrants (Chinnery 1965, Bilham & King 1989) occurs near the terminations of strike-slip faults. Near the upper or lower periphery of a strike-slip fault (mode III crack tips), echelon fracture arrays may develop (Pollard *et al.* 1982, Cox & Scholz 1988, Jackson *et al.* 1992). A wide range of 'mixed-mode' conditions along the periphery of a fault may lead to more complex deformation patterns (Pollard & Segall 1987). This study addresses lateral (mode II) fault terminations and stepovers that show no evidence of significant mode III deformation.

Individual fault segments typically display a left- or right-stepping echelon geometry. Echelon geometries may stem from pre-existing arrangements of weak surfaces (e.g. joints, bedding planes, and older faults) or may develop during shearing (Gamond 1987, Swanson 1988). The interaction of fault segments leads to characteristic stress fields and deformation patterns, depending on the sense of fault stepover vs the sense of shear of the fault zone (Segall & Pollard 1980).

We would prefer to refrain from the common usage of stress or strain terms to describe fault stepovers (see Scholz 1990, for a review of terminology and additional references), because the complex stress and strain fields about a fault step of either geometry always include zones of tension or extension and compression or contraction (Segall & Pollard 1980). However, to avoid cumbersome geometric phrases, we adopt the use of *extensional step* for left steps along left-lateral faults and right steps along right-lateral faults, and *contractional step* for the contrasting cases.

Joints, veins, dilation breccias, extensional faults, or regions of stretched rock typically link fault segments adjoining the extensional step. Extensional fault steps occur along millimeter-scale shear zones in felsic gneiss (Gibson 1990), in outcrops in a variety of rock types (e.g. Granier 1985, Gamond 1987, Swanson 1988, Cruikshank *et al.* 1991), along mine-induced meter-scale faults (McGarr *et al.* 1979, Sibson 1987), and along large strike-slip fault zones such as the San Andreas fault where sag ponds and basins mark the fault stepovers (e.g. Crowell 1974a,b, Christie-Blick & Biddle 1985, Woodcock & Fischer 1986). Analogue models of echelon faults in a variety of materials produce similar structures (Brace & Bombolakis 1963, Tschalenko 1970, Hempton & Neher 1986, Naylor *et al.* 1986, Lin & Logan 1991). In all cases mass is removed from the fault step as slip on the bounding faults continues. The resulting mass loss may be compensated by the emplacement of mineral precipitates into veins or rhombochasms (Sibson 1987), by contraction across the step perpendicular to the faults (Woodcock & Fischer 1986), or by vertical contraction commonly leading to basin formation along crustal fault systems (Crowell 1974a, Dibblee 1977).

Contractional steps are characterized by shortening sub-parallel to the fault planes within the step. As material is pushed into the step, possible accommodating mechanisms include diffusive mass transfer (Gamond 1987, Martel *et al.* 1990), extension perpendicular to the step-bounding faults and distortion of the fault planes (Woodcock & Fischer 1986), or extension in the vertical direction. The latter commonly results in uplift along crustal-scale strike-slip faults (Sharp & Clark 1972, Dibblee 1977, Woodcock & Fischer 1986).

*Brittle–ductile deformation*

A 'brittle-to-ductile transition' does not directly imply the deformation mechanisms involved (Paterson 1978, Rutter 1986, Ross & Lewis 1989). Therefore, seismologists, structural geologists, and rock mechanicists commonly have different views as to the nature of this transition (e.g. Byerlee 1968, Smith & Bruhn 1984, Simpson 1985, Sibson 1986a, Scholz 1988, Tullis 1990). Here, we consider a brittle–ductile transition to reflect a material state (range of temperature, deformation rate, finite strain and stress conditions) beyond which the activation of crystal–plastic dislocation creep, dynamic recrystallization, and/or diffusive mass transfer of one or more mineral constituents allows the rock to flow macroscopically. Below the transition a material will fail predominantly by brittle fracture if its strength is exceeded.

We infer past 'ductility' in deformed rock if we ob-

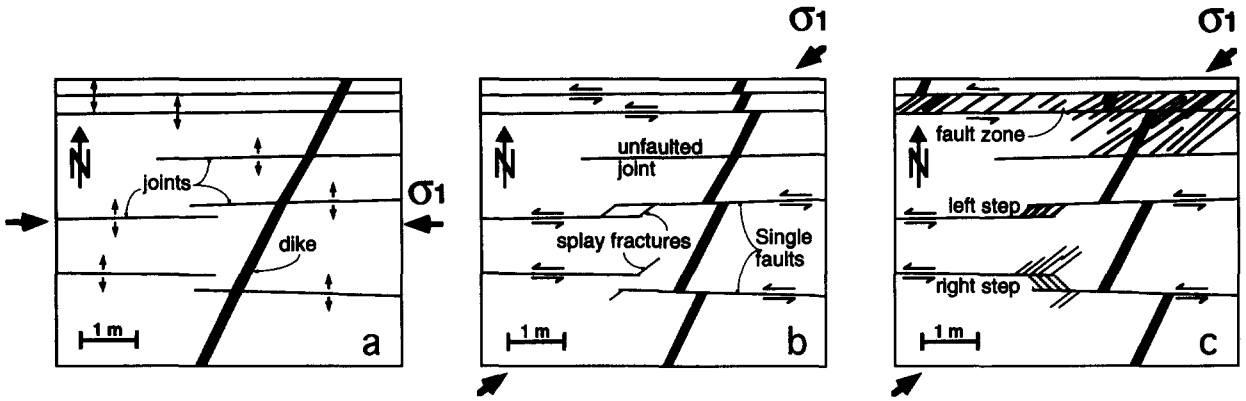


Fig. 2. Map views of Late Cretaceous development of joints and faults in the Mt. Abbot quadrangle. (a) Joints formed soon after emplacement of the Lake Edison Granodiorite. (b) Stress reorientation subsequently caused left-lateral fault slip along the joint planes and splay fractures form near fault terminations. (c) Individual faults interact across left and right steps and form brittle fault zones. Ductile deformation occurs in contractional right steps and dilatant fracturing in extensional left steps and in the fault zones (after Segall & Pollard 1983a,b, Martel *et al.* 1989).

serve abundant microstructures such as undulatory extinction, a preferred orientation of *c*-axes, recrystallized grains, or pressure solution seams (Simpson 1985). We infer past 'brittle' behavior if we observe few of the above microstructures and instead find that fracture was the dominant deformation mechanism. However, both brittle and ductile structures can form over a wide range of conditions (e.g. Scholz 1988, Swanson 1992). A transition to crystal–plastic deformation in experiments can be achieved by increasing temperatures, by the addition of water, by applying high confining pressures, and by decreasing strain rates (e.g. Tullis & Yund 1977, 1980); it is furthermore dependent in a more complex fashion on the state of stress, as will be discussed below.

## STRUCTURAL DEVELOPMENT OF FAULT ZONES IN THE LAKE EDISON GRANODIORITE

In the Late Cretaceous, fine- to medium-grained biotite–hornblende Lake Edison Granodiorite (Bateman 1992), early ENE-striking joints are mineralized with epidote, chlorite ± quartz ± biotite ± sphene ± calcite ± zeolites (Segall & Pollard 1983a, Segall *et al.* 1990). Some of these joints were later reactivated as left-lateral strike-slip faults (Segall & Pollard 1983b) (Fig. 2b). The coexistence of parallel faulted and unfaulted mineralized joints shows that the fault surfaces did not form as shear but as dilatant fractures (Segall & Pollard 1983b). Therefore, the initial geometry, spacing and orientation of faults is not related to the later shearing event. Offsets along the faulted joints range from millimeters to 2 m, and fault segments range from a few meters to several tens of meters in length. A strong mylonitic fabric in fine-grained chlorite, epidote and quartz along fault zones indicates that crystal–plastic deformation accommodated fault slip. Sharp boundaries commonly separate fault rocks from wall rocks, but some grains were plucked from the granodiorite wall and sheared during fault slip. Individual faults did not extend beyond the terminations of the older joints (Segall & Pollard 1983b).

Some parallel faults form fault zones (Fig. 2c) about 1 m in width that accommodate up to several tens of meters of slip on their bounding surfaces (Segall & Pollard 1983b, Martel *et al.* 1988, Martel & Pollard 1989). In these boundary faults the mylonitic fabric has a cataclastic overprint. Martel *et al.* (1988) postulated that the transition from mylonitic fabrics in smaller faults to cataclastic textures in boundary faults that accommodated larger displacements resulted from an increase in the shear strain rate across the boundary faults as adjacent faults became inactive. Alternatively, the cataclastic deformation may be related to cooling of the pluton as deformation progressed (Christiansen *et al.* 1992).

Two radiometric ages bracket the age of faulting. The Lake Edison Granodiorite is ~85–90 Ma based on U–Pb ages of zircon (Stern *et al.* 1981). Muscovites grown during hydrothermal alteration in the fractured interiors of two ENE-trending left-lateral fault zones yield $^{40}Ar/^{39}Ar$ and K–Ar dates of 75–79 Ma (Segall *et al.* 1990), which is a minimum age of motion along these faults. Thus jointing and slip on individual faults must have occurred within a 6–15 Ma interval.

Jointing presumably occurred during the initial cooling and dewatering (Best 1982, p. 290) of the Lake Edison Granodiorite. Subsequent stress reorientation and faulting may be related to the intrusion of the neighboring, somewhat younger Mono Creek Granite to the east (Bateman 1992) (Fig. 1). The increased development of ductile fabrics along the faults near the younger pluton may indicate that faulting occurred during or soon after intrusion of the Mono Creek Granite (Segall *et al.* 1990). However, the abundance of similarly oriented fracture sets throughout the central Sierra Nevada (Mayo 1941, Lockwood & Moore 1979) and evidence of significant margin-parallel right-lateral shear in the Late Cretaceous (Page & Engebretson 1984, Busby-Spera & Saleeby 1990, Tikoff & Teyssier 1992) suggest a relationship to regional tectonism (Davies & Pollard 1986, Segall *et al.* 1990).

The wall rock adjoining some joints was altered by interaction with circulating fluids, resulting in albitization of calcic-plagioclase and K-feldspar within several

centimeters of the joints. Sericitization of feldspar, removal of mafic minerals and an abundance of fluid inclusions give the altered rock a bleached appearance (Segall *et al.* 1990). These alteration halos increase in width where joints intersect (Segall & Pollard 1983a). Quartz veins and alteration of wall rock at fault terminations, in extensional steps and bends, and within fault zones suggest that fluid flow also accompanied the development of the linked fault systems.

Structures formed during faulting in the Lake Edison Granodiorite were both brittle and ductile in nature (Segall & Simpson 1986, Bürgmann & Pollard 1992). Kronenberg *et al.* (1990) described the first natural example of localized hydrolytic weakening where ductile shearing spreads from a fault segment in the Lake Edison Granodiorite. They observed a correspondence of water concentrations in quartz (mostly in fluid inclusions) and ductilely accommodated shear strain in the rock adjacent to the fault. This suggests that water infiltration through open microcracks during initial jointing may have induced a reduction in ductile strength of the wall rock (Kronenberg *et al.* 1990). Bürgmann & Pollard (1992) suggested that there is a mean-stress dependent transition from brittle deformation processes to crystal–plastic deformation in quartz and mica within contractional fault steps.

## FAULT TERMINATIONS

Three fundamentally different types of fault terminations developed in the Lake Edison Granodiorite at different distances from the neighboring Mono Creek Granite: (1) fault terminations with splay fractures (Figs. 3a & b), (2) fault terminations with splay fractures and mylonitic fabrics juxtaposed on either side of the fault (Fig. 3c), and (3) fault terminations with mylonitic fabrics ahead of the fault terminations (Fig. 3d). We hypothesize that these structures reflect the material response of the granodiorite at different temperatures as the neighboring pluton reheated the Lake Edison Granodiorite.

The first type of fault termination with dilatant splay fractures in the NE and SW quadrants oblique to the left-lateral faults (Figs. 3a & b) occurs throughout the pluton. Little or no shear offset is observed on splay fractures formed at angles ranging from about 30–60° to the faults. Commonly a set of fractures spaced several centimeters apart forms near the fault termination. Continued opening of splay fractures in the presence of hydrothermal fluids allows the formation of thick wedges filled with precipitates, primarily quartz (Fig. 3a). There is no evidence of ductility in the granodiorite in the vicinity of these fault terminations. However, mylonitic fabrics in the fine-grained fault material and deposition of quartz, epidote and chlorite in the splay fractures indicate that deformation occurred during hydrothermal activity. Splay fractures provided efficient conduits for fluid flow during faulting.

Closer to the Mono Creek Granite are fault terminations with mylonitic fabrics in the quadrants opposite to splay fractures (Fig. 3c). In Fig. 3(c), the slip gradient near the fault termination is very steep; slip decreases from about 0.8 m to 0 m in <2 m. Significant strain in the granodiorite accommodates the slip gradient along the fault.

Within about 100 m of the contact with the Mono Creek Granite, some faults terminate in localized zones of mylonite up to a meter wide that do not extend more than a few meters from the fault ends. Figure 3(d) shows two dikes in the vicinity of a fault termination. One dike about 1.5 m behind the fault termination is offset by ~1.2 m across the fault, whereas a second dike 0.5 m ahead of the fault termination is strongly sheared and thinned but not offset. As slip on the sheared joint decreases rapidly towards the termination, the zone of deformation broadens from a few millimeters into a continuous shear zone about 70 cm across.

## EXTENSIONAL STEPS

Where two faults are arranged in an echelon geometry, the brittle and/or ductile strain intensifies due to fault interaction. We mapped several left and right steps in detail to determine the geometries of the structures and to examine the deformation mechanisms accommodating the strain.

Numerous veins filled with quartz, epidote and chlorite formed in extensional steps, indicating significant local dilation that accommodates slip transfer between the fault segments. In addition the host granodiorite in extensional steps is extensively altered by hydrothermal fluids. The size of fractured left steps ranges from a few centimeters to ~1 m in width and up to 2 m of overlap. Vein thicknesses of up to 10 cm can be found in some steps.

Figure 6 shows an extensional stepover at site HE90 located about 350 m from the Mono Creek Granite (see Fig. 1). The 7 cm offset of an aplitic dike across the eastern stepover-bounding fault compares well with the combined opening of 5–6 cm within the stepover determined from the vein widths measured at varying distances from the faults. This comparison demonstrates that macroscopic dilatant fractures have transferred at least 70% of the slip across the stepover. Even though the fracture of the eastern fault segment continues for 2 m to the west of the stepover it shows no evidence of fault slip past the stepping region. Two NE-striking mineralized fractures initiate on the eastern fault segment outside of the fault stepover. These fractures are splay fractures from the western segment that cut across the eastern segment, suggesting that slip on the latter was of lesser magnitude. Several NS-striking joints with no mineral filling or associated alteration zones are not related to faulting. There is no evidence of ductile fabrics associated with extensional steps; deformation is purely brittle by dilatant fracture between the fault stepovers.

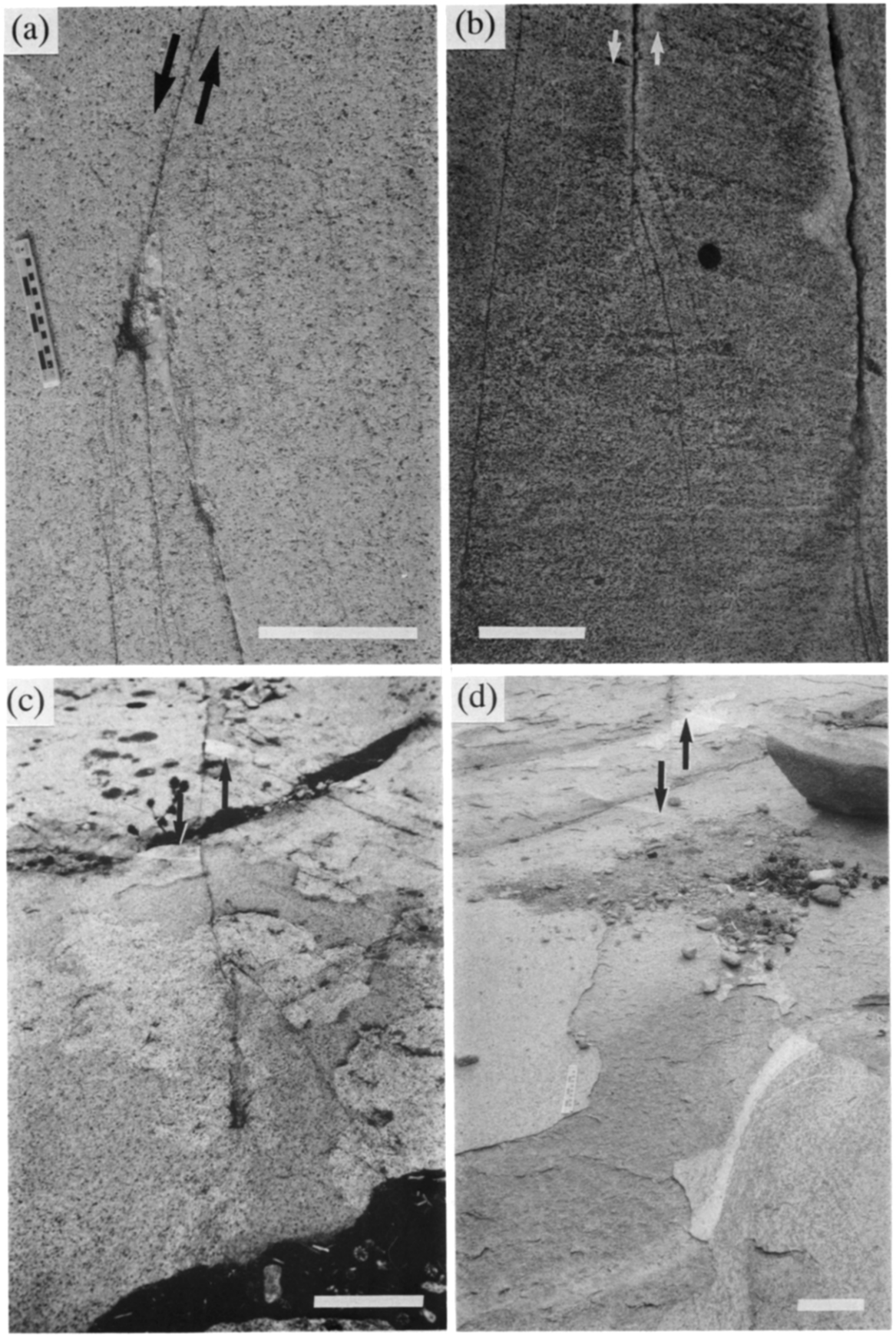


Fig. 3. Fault-termination structures in the Lake Edison Granodiorite observed at various distances from the neighboring Mono Creek Granite. (a) & (b) Splay fractures in extensional quadrant; the wedge near the fault termination in (a) is filled with quartz. (c) Splay fractures in extensional quadrant and mylonitic fabric in the contractional quadrant. (d) Symmetric mylonitic shear zone spreading from fault termination. Arrows in (c) & (d) point to offset aplite dikes indicating meter-scale slip magnitudes near fault terminations. Scale bars are 20 cm.

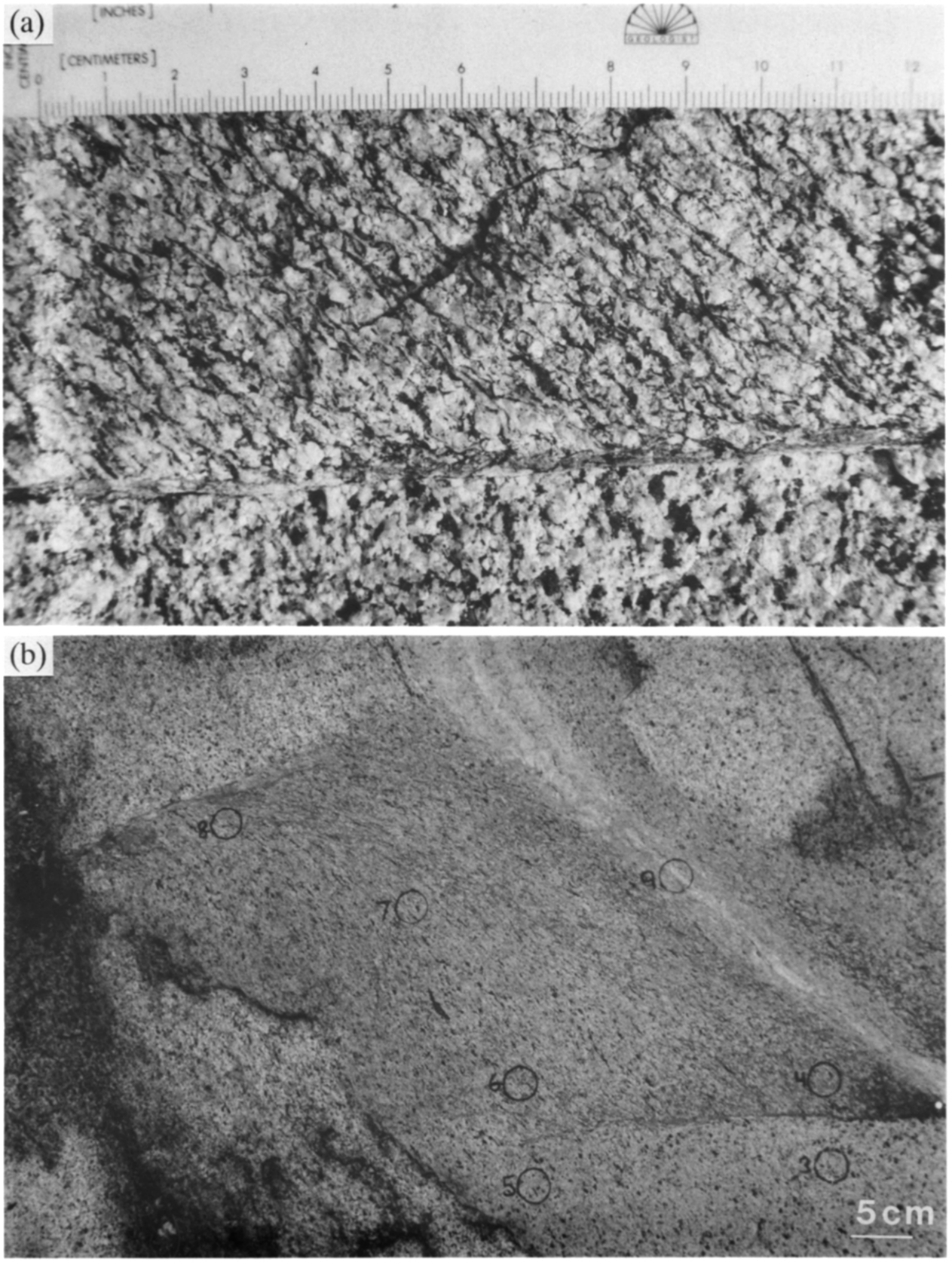


Fig. 4. (a) Close-up photograph of fabric contrast across the step-bounding fault in boxed region near core 12 in Fig. 7. (b) Close-up photograph of contractional step in upper panel of Fig. 8 showing a marked textural change (isotropic to foliated) across the step-bounding faults. The aplite dike is thinned to 2–3 cm in the stepover from an original thickness of 14 cm and reoriented by counterclockwise rotation of ~35°. The numbered circles mark the location of core samples taken for microstructural and geochemical analysis.

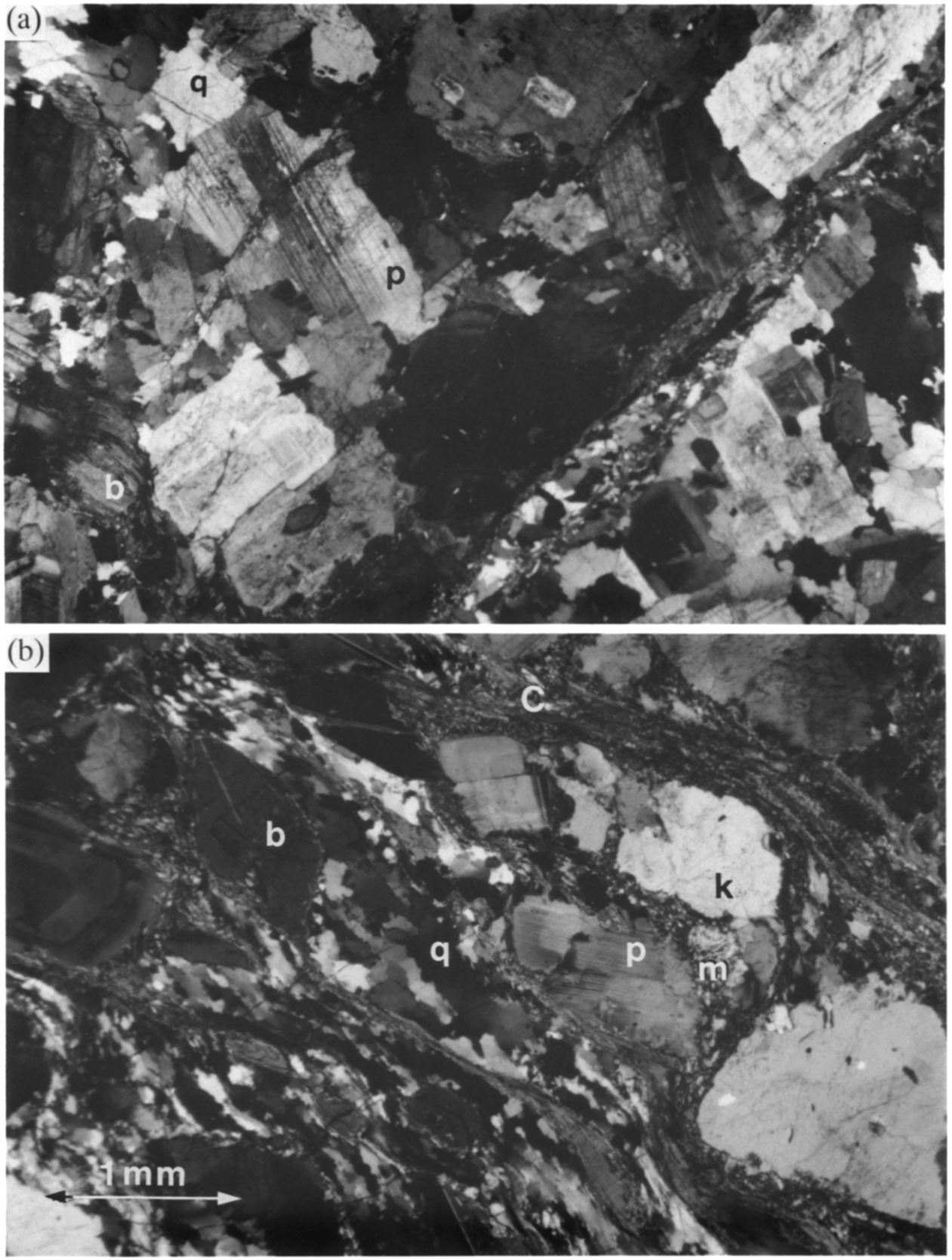


Fig. 5. Photomicrographs of thin sections from cores 6 and 8 under crossed nichols (see Fig. 7 for core locations). Both photographs are at the same magnification. (a) Core 6 (located 10 cm away from the step) showing dilatant fractures filled with quartz and no fabric development. (b) Core 8 from ductilely deformed step area showing recrystallized quartz, fractured feldspars, mica fish textures, and *S-C* type fabrics indicative of non-coaxial flow. C—mylonitic C-surface, b—biotite, k—potassium feldspar, m—myrmekite, p—plagioclase, q—quartz.

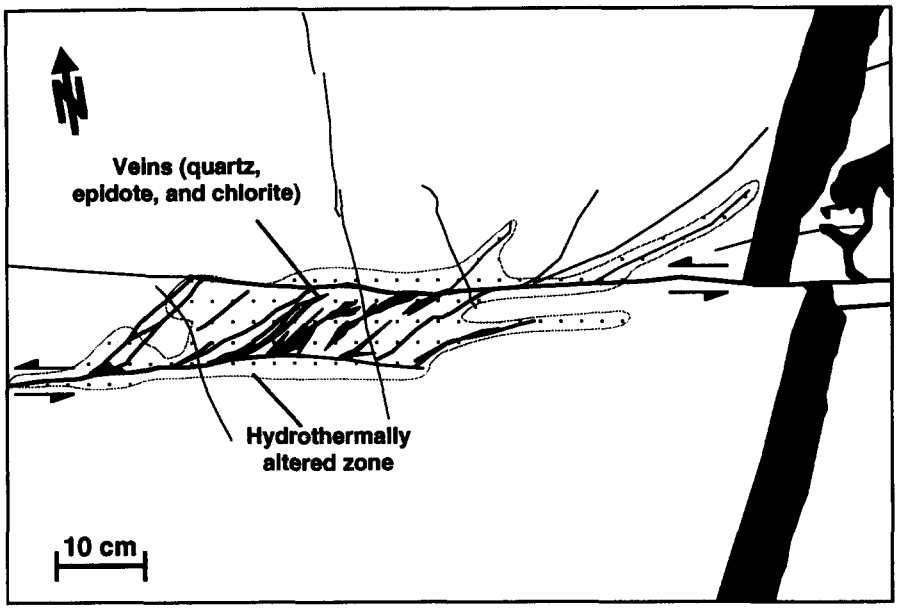


Fig. 6. Outcrop map of two extensional step echelon fault segments at site HE90 linked by dilatant fractures that transfer 5–6 cm of slip between the faults. Note bleached halo of altered granodiorite indicating active fluid circulation through the step. The fault-linking veins are filled with quartz, minor chlorite and epidote.

## CONTRACTIONAL STEPS

### *Macroscale structure*

Figure 7(a) shows an outcrop map from the Bear Creek area labeled BA90 in Fig. 1 that is located 1.5 km from the Mono Creek Granite (Bürgmann & Pollard 1992). The EW-striking fractures have apparent slip magnitudes from a few centimeters to more than a meter determined from the offsets of a NW-striking aplite dike and mafic xenoliths. Slickensides measured along several of the faults plunge <10° to the east, indicating that displacements on the faults are approximately left-lateral strike-slip. Dilatant splay fractures oriented at angles of 30–60° from the faults are associated with fault stepovers and bends along the faults. A weekly developed fabric defined by elongated grains parallel to the orientation of flattened xenoliths trends approximately 315° (Fig. 7a). This fabric predates the formation of joints and faults and probably formed during the early cooling of the pluton.

The rock outside of the contractional steps shows no evidence of significant ductile strain. A zone of NE-striking fractures in the middle left of Fig. 7(a) is spatially related to the fault stepover shown in detail in Fig. 7(b), forming a large splay fracture array. The mineral-filled fractures oriented 50–60° to the faults accommodate some extension. The 1.2 m offset of the aplite dike located 3–4 m to the west of the fault stepover is reduced by about 6–8 cm by the combined dilation of about 60 mineralized splay fractures between the offset dike and the fault termination.

Well-developed ductile fabrics, shown as hachured areas, are restricted to contractional steps along the faults. Only millimeters outside the steps, the granodiorite is approximately isotropic (Fig. 4a). *S–C* mylonites (Lister & Snoke 1984) within the stepover indicate a component of non-coaxial flow. The *S* foliation is oriented 25–35° to faults close to them and oriented 40–55° to faults in the center of the fault stepover (Fig. 7b). Distinct shear surfaces (*C*-planes), that can be recognized throughout much of the foliated zone are oblique to the fault strike by up to 15° (Fig. 7b).

Figure 8 is a map of a sequence of echelon fault segments at outcrop HB90 in Fig. 1, located 360 m from the Mono Creek Granite. Slip has been transferred effectively across five contractional stepovers. The offsets of aplite dikes across the fault segments increase from east to west independent of the size of the individual fault segment (Fig. 8). The stepover zones between echelon fault segments are up to 1.5 m wide.

One of the aplite dikes crosses the contractional step labeled HB90 in Fig. 8. The fault step is about 30 cm wide and the faults overlap by 5 cm (Fig. 4b). The dike dips 75–80° to the southwest within the fault stepover and is approximately vertical several meters from the stepover. The dike is offset by 76 cm along the eastern fault segment and is thinned from 14 cm to 2–3 cm and rotated counterclockwise by about 35° within the fault stepover (Fig. 4b). This corresponds to an offset of 1.15 m of a second dike on the western fault segment, indicating that the slip was transferred almost in full across the stepover. Both faults curve outward adjacent to the step, indicating an outward bending of the faults as material is pushed into the stepover. However, the widening of the stepping region cannot accommodate the horizontal shortening of about 1 m we infer from the fault offsets. The thinning of the aplite dike in the step indicates that up to 80% of the rock originally located within the fault step had to be removed to accommodate slip transfer.

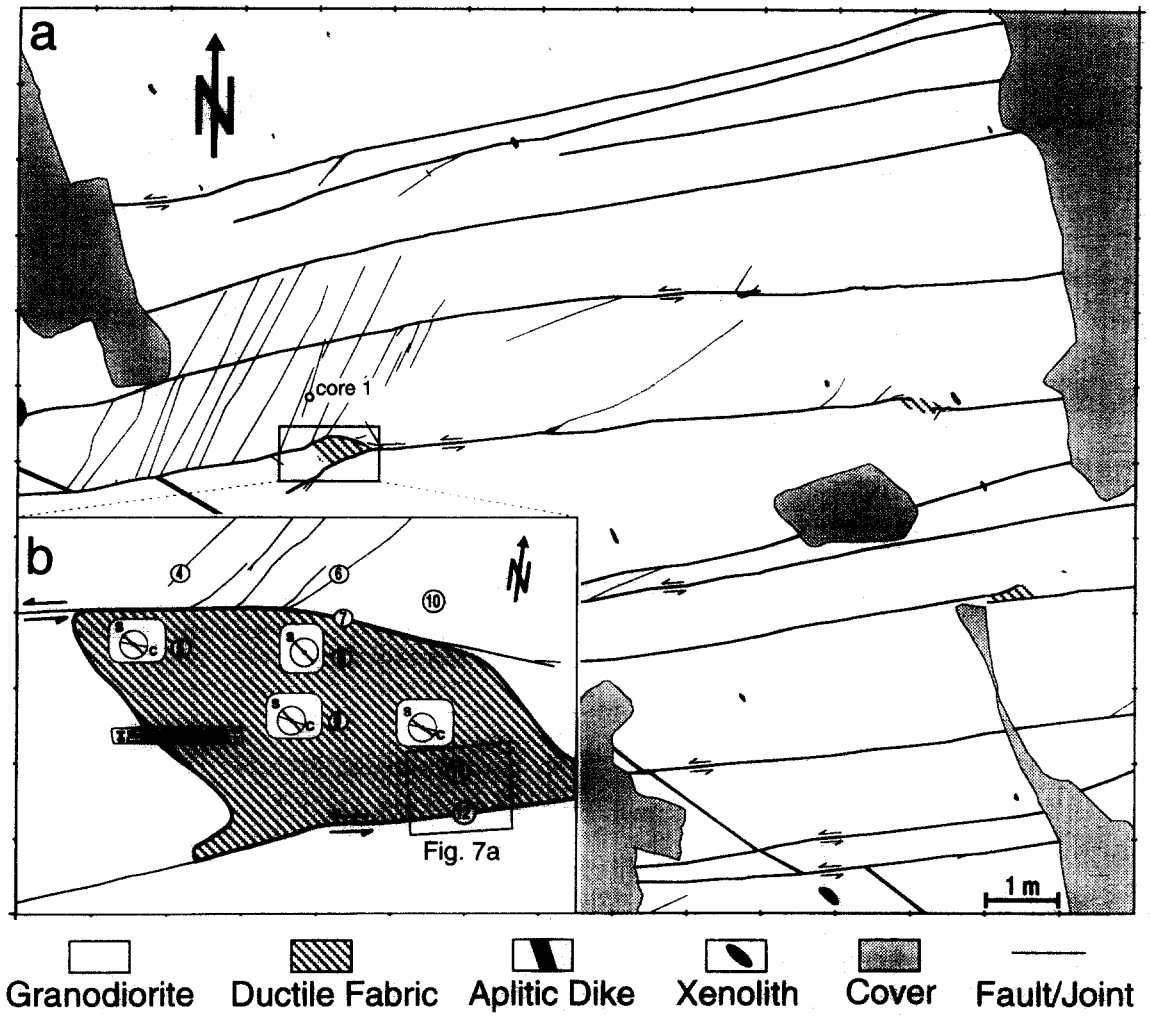


Fig. 7. (a) Outcrop map of faults, fractures and right steps at location BA90 in Fig. 1. Left-lateral offsets on some of the faults are indicated by a displaced aplite dike. Oblique fractures near the boxed contractional step appear to be related to stress perturbations near the fault step. (b) Detailed map of boxed right step. Circled numbers indicate core sample location. Diagrams show the orientation of *S* and *C* planes in thin sections from cores.

*Microscale structure*

We analyzed several thin sections to characterize the deformation of the granite around the stepover BA90 in Fig. 7(b). Core 6 (see location in Fig. 7b) has an approximately isotropic fabric and quartz shows only slight undulatory extinction (Fig. 5a). Grain diameters are typically 1–3 mm. A splay fracture emanating from the step-bounding fault crosses the lower-right of the photograph. Grain-scale faults at various orientations and dilatant fractures oriented subparallel to the splay fractures are common in feldspars. Deformation is brittle, dominated by dilatant fracturing of an interconnected feldspar framework.

In core 8 (Fig. 5b) from within the contractional stepover (Fig. 7b), quartz grains are dynamically recrystallized and strongly elongate, indicating crystal–plastic flow. Biotite, often altered to chlorite, is also crystal–plastically deformed and shows typical 'mica fish' textures (Lister & Snoke 1984). Myrmekites that are common in the undeformed granodiorite are often crushed and deformed by cataclastic flow of feldspars in a matrix of fine-grained quartz. Distinct, EW-striking shear surfaces (*C*-planes), rich in fine-grained mica and finely recrystallized quartz, separate zones of feldspars and plastically deformed quartz and biotite. The quartz and biotite domains anastomose in and out of the *C*-planes and wrap around feldspar clusters that are elongate parallel to the macroscopic foliation (*S*-planes) and oblique to the *C*-planes and the stepover-bounding faults. Feldspar grains are commonly deformed by extensional cracks, shear fractures along cleavage planes, and cataclastic flow at grain boundaries. Patchy undulatory extinction in some feldspar grains is interpreted to be due to submicroscopic cataclasis (Tullis & Yund 1987). Overall, deformation is ductile, dominated by crystal–plastic flow of quartz and mica enveloping grains of broken feldspar, hornblende and opaques.

Figure 9 shows maps of plagioclase, K-feldspar, quartz and opaque minerals of cores 1 and 9 (see Fig. 7 for core locations). We were able to accurately calculate the area percentage of the individual mineral constituents. Individual grain boundaries between neighboring grains of the same mineral species, however, could not be mapped.

The textures in the horizontal section from core 1,

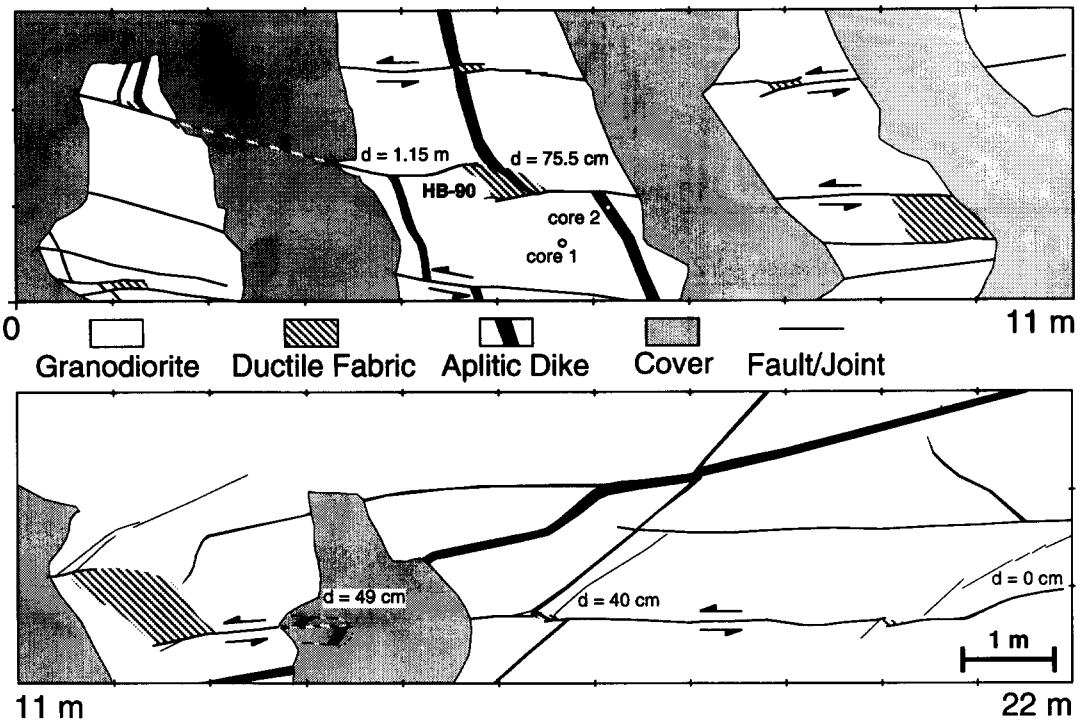


Fig. 8. Outcrop map of faults, fractures and contractional right steps at location labeled HB90 in Fig. 1. Fault-slip measurements are from offset aplite dikes.

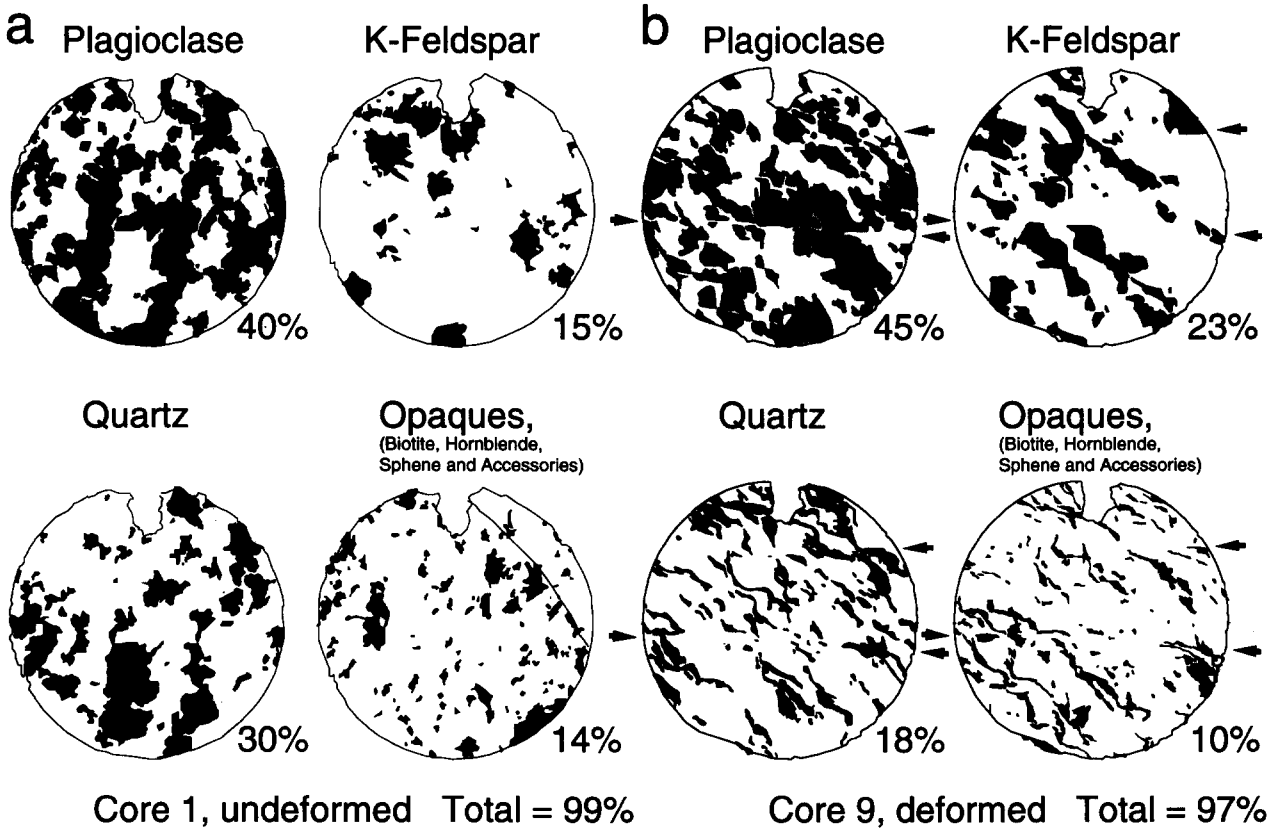


Fig. 9. Thin section maps of quartz, feldspars and opaques in cores 1 and 9 (see Fig. 7 for core location). The diameter of the cores is 2.54 cm, the notches at the tops of the sections are oriented towards the north. Both feldspars were stained on the thin section to allow easy recognition on an image projected onto a digitizing table. (a) The fabric in core 1 is approximately isotropic. (b) The granodiorite in core 9 is strongly sheared; grains are elongated in the NW–SE direction and are dragged along EW-striking *C*-planes. Note the reduced quartz content of core 9 compared to core 1.

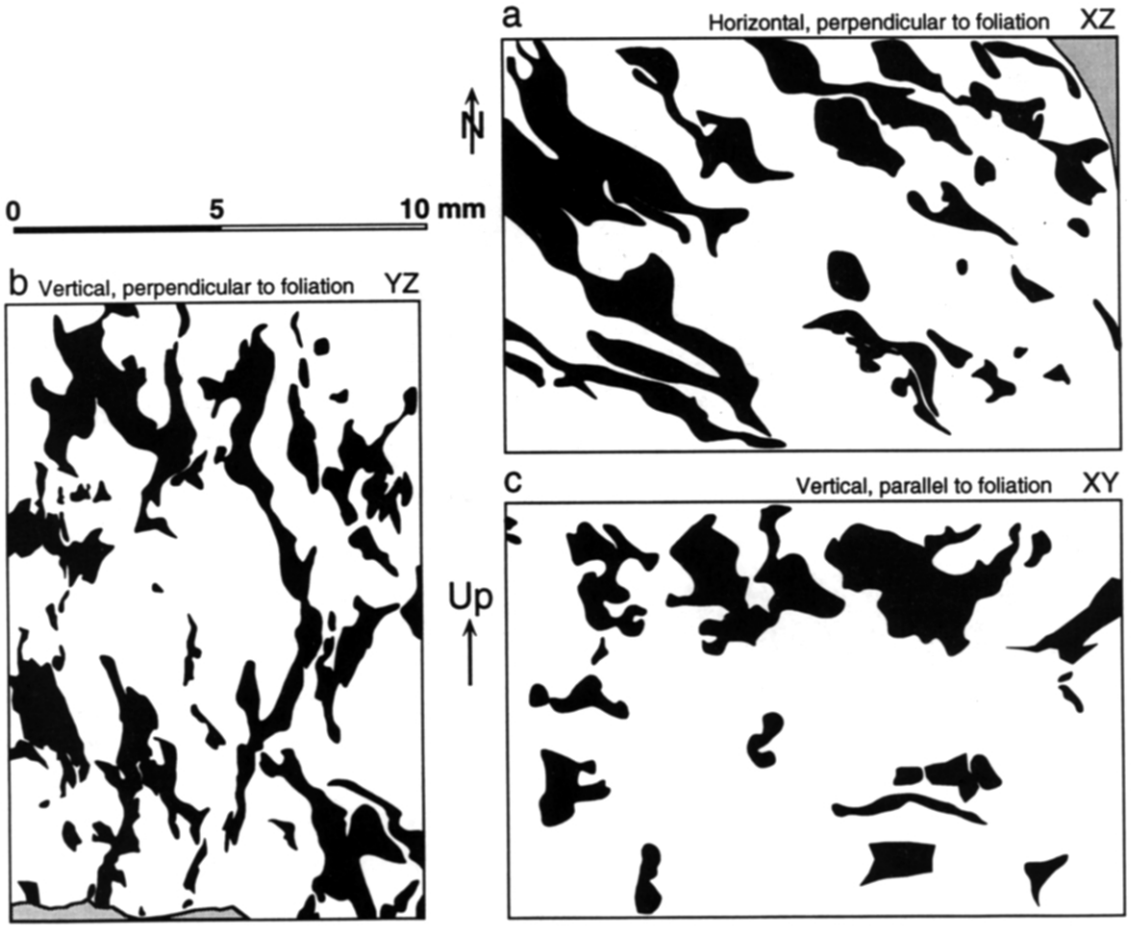


Fig. 10. (a)–(c) Three mutually perpendicular thin section maps of quartz domains for core 8 from within the stepover at outcrop HB90 [Fig. 8, see Fig. 4(b) for core location]. The foliation is defined by deformed elongate quartz aggregates. Note that the quartz domain shapes in the foliation plane in (c) are approximately equant.

located about 1 m north of the fault step, indicate that the little-deformed granodiorite is characterized by an interconnected framework of feldspar interspersed with approximately equant-shaped quartz, amphibole and biotite grains (Fig. 9a). A weakly developed, approximately NS-oriented elongation of feldspar and quartz grain aggregates follows the trace of the regional foliation.

The foliated granodiorite from core 9, taken from the middle of the step, shows drastically different textures (Fig. 9b). Feldspar grains are aligned and slightly elongated in a NW–SE orientation. The feldspar framework apparent in core 1 is broken, and thin bands of flattened quartz and mica domains envelop the feldspar grains. The quartz bands and mica domains curve into two EW-striking shear surfaces in the middle and upper half of the section.

Thin sections were cut along three mutually perpendicular planes, parallel and perpendicular to the foliation plane, to evaluate the three-dimensional strain and the distribution of strain within a fault stepover (Fig. 10). Most cores were used for the geochemical analysis (see below), so we do not have a complete picture of textural changes throughout the fault step. Quartz-aggregate shapes from core 8 in Fig. 7(b), located about 2 cm from the step-bounding fault, display (1) sigmoidal patterns indicating non-coaxial shear in the horizontal plane (Fig. 10a), (2) strongly stretched grain aggregates in the vertical plane perpendicular to foliation (Fig. 10b), and (3) approximately equant grain shapes in the foliation plane (Fig. 10c). In core 4 in Fig. 7(b), grain shapes also suggest a finite strain ellipsoid that is flattened oblique to the bounding faults with $X$ and $Y$ axes of subequal length. Indicators of non-coaxial strain such as mica fish, sigmoidal grain shapes, and $SC$-fabrics show that the strain has a strong simple-shear component.

*Diffusive mass transfer: mineralogic and geochemical analyses*

Mineralization in dilatant fractures associated with the faults is common. The source of the precipitating material is not obvious, however. Diffusive mass transfer may have occurred only over short distances at the grain scale, but the large volume of some of the vein fillings suggests otherwise. Fluids may have been derived from a magmatic source, possibly from the newly intruded, cooling Mono Creek Granite to the east. Diffusive mass transfer may also have occurred locally, possibly involving mass removal from the deformed contractional steps. As the mineralizations in splay frac-

Table 1. Geochemical analysis of samples from outside and within contractional fault steps

| Cores | BA90-1 & 3 Undef. | BA90-4, 6 & 10 Undef. nearby | BA90-8, 9 & 11 Def. | HB90-1, 3 & 5 Undef. | HB90-7, 4 & 8 Def. | HC90-1, 2, 7 & 9 Undef. | HC90-6 & 10 Def. | 1 Sigma (G-2)* | Precision (%)‡ |
|---|---|---|---|---|---|---|---|---|---|
| Major Elements (%) | | | | | | | | | |
| $SiO_2$ | 65.86 | 66.22 | 65.94 | 70.48 | 69.15 | 66.76 | 66.29 | 0.35 | 0.13 |
| $TiO_2$ | 0.55 | 0.53 | 0.51 | 0.36 | 0.39 | 0.54 | 0.53 | 0.01 | 0.00 |
| $Al_2O_3$ | 16.07 | 15.82 | 15.71 | 15.01 | 14.89 | 15.71 | 16.01 | 0.11 | 0.06 |
| $Fe_2O_3$ | 4.25 | 4.23 | 4.11 | 2.97 | 2.98 | 4.05 | 3.99 | 0.02 | 0.02 |
| MnO | 0.08 | 0.08 | 0.08 | 0.07 | 0.07 | 0.08 | 0.08 | 0.00 | 0.00 |
| MgO | 1.83 | 1.81 | 1.80 | 1.14 | 1.15 | 1.52 | 1.53 | 0.01 | 0.01 |
| CaO | 4.38 | 4.28 | 4.09 | 2.98 | 3.07 | 3.84 | 3.85 | 0.01 | 0.00 |
| $Na_2O$ | 3.59 | 3.49 | 3.46 | 3.45 | 3.67 | 3.77 | 4.07 | 0.06 | 0.03 |
| $K_2O$ | 3.04 | 3.17 | 3.36 | 4.08 | 3.41 | 3.18 | 2.87 | 0.03 | 0.01 |
| $P_2O_5$ | 0.18 | 0.17 | 0.17 | 0.12 | 0.13 | 0.20 | 0.20 | 0.00 | 0.00 |
| Total | 99.83 | 99.79 | 99.22 | 100.66 | 98.92 | 99.65 | 99.41 | 0.40 | 0.56 |
| Trace Elements (ppm) | | | | | | | | 1 Sigma (G-2)† | Precision (ppm)‡ |
| Zr | | 111.7 | 114.0 | 97.4 | 95.4 | | | 1.99 | 3.34 |
| Y | | 10.3 | 9.5 | 6.8 | 7.5 | | | 0.64 | 0.36 |
| Nb | | 9.4 | 9.7 | 6.9 | 8.7 | | | 0.26 | 0.14 |
| Sr | | 540.4 | 532.6 | 443.4 | 447.2 | | | 2.14 | 2.52 |
| U | | 6.4 | 7.1 | 3.2 | 4.0 | | | 0.67 | 0.35 |
| Rb | | 132.3 | 137.0 | 147.0 | 164.2 | | | 0.55 | 0.79 |
| Th | | 17.4 | 16.1 | 15.5 | 16.9 | | | 0.65 | 0.63 |
| Pb | | 18.4 | 18.8 | 22.8 | 22.4 | | | 0.94 | 0.26 |
| Ga | | 17.8 | 16.6 | 16.2 | 17.3 | | | 0.29 | 0.38 |

*Standard deviation of 14 G-2 standard analyses over 5 days.
†Standard deviation of 4 G-2 standard analyses over 8 days.
‡Mean of standard deviations of own repeated samples.

tures and along some fault segments are mostly quartz, we would expect a reduction of silica content in the deformed rock.

To test the hypothesis of local mass removal by diffusive mass transfer in areas of ductile fabric development, we determined the modal mineralogy from thin sections and carried out a geochemical analysis of major and minor elements of deformed and undeformed granodiorite. By mapping out the mineral distribution in a thin section we can test for selective removal or concentration of individual mineral species. The modal analysis, based on area percentage of the mapped mineral constituents in Fig. 9, indicates a large decrease of quartz from 30% in the undeformed core 1 to 18% in the deformed core 9. Increased concentrations of micaceous material along discrete shear surfaces (*C*-planes) oblique to the shortening direction suggest that pressure solution may have occurred in these high strain zones.

However, the modal mineralogies deduced from 2.5 cm-diameter thin sections are based on a very small sample size. Therefore, we undertook major-element analyses of cored samples from the two fault stepovers at BA90, HB90 and a third site, HC90 (about 150 m E of HB90), as well as trace-element analyses for BA90 and HB90. Geochemical analyses of cored samples can determine if bulk chemical differences exist between deformed and undeformed samples and can test for the removal or residual enrichment of mobile and immobile elements, respectively. Table 1 indicates which cores were used in the X-ray fluorescence spectroscopy analyses and shows the results and the associated uncertainties.

To determine the extent of diffusive mass transfer, we compare the concentrations of $SiO_2$ and the immobile elements $TiO_2$ and Zr (e.g. Ague 1991). Figure 11 shows the ratios of the concentrations in the deformed samples ($C_s$) and the approximately undeformed cores ($C_o$). While the concentration of $SiO_2$ in the fault stepovers is less than or equal to that of the undeformed rock in each sample, the differences of less than 1.5% are not significant. $TiO_2$-concentration differences are also in the range of the analytical errors, and show no consistent trend of enrichment or reduction. This holds true for Zr as well.

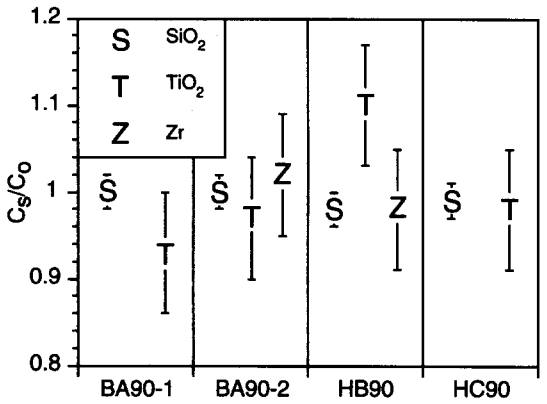


Fig. 11. Concentration ratios of $SiO_2$, $TiO_2$ and Zr between undeformed and deformed samples derived from Table 1. (See Fig. 1 for sample locations, HC90 is located ~200 m NE of HB90.) Significant differences in concentrations of mobile or immobile elements between deformed and undeformed samples are not apparent.

The results do not indicate any significant decrease of mobile phases or enrichment of immobile elements due to mass removal by diffusive mass transfer. It is interesting to note, however, that a comparison of samples from the individual sites suggests volume strains of up to 30%

(calculated after Ague 1991), indicating significant heterogeneity in the rock composition over a few hundred meters. We conclude that while diffusive mass transfer may have occurred at the grain scale and is clearly implicated in the abundant mineral precipitation in the area, the mineral constituents were not derived from ductilely-deforming stepover zones along the faults. The quartz-content change observed in the thin sections in Fig. 9 reflects the natural heterogeneity of the rock at the thin-section scale and not diffusive mass transfer.

In summary, we find that strain in mylonitically-deformed contractional steps in the Lake Edison Granodiorite apparently was accommodated by ductile flow, including a vertical flow component. Diffusive mass transfer was not responsible for the significant mass transport out of the contractional steps required by their kinematics.

## TEMPERATURE-DEPENDENT DEFORMATION STYLE AT FAULT TERMINATIONS

Deformation was increasingly accommodated by ductile mechanisms as the contact to the neighboring Mono Creek Granite is approached. This pluton is younger than the Lake Edison Granodiorite and apparently intruded during faulting. The enhanced ductility near its contact is evidenced by steep slip gradients near fault terminations, ductile slip transfer across more widely-spaced right-stepping faults, and the development of symmetric ductile shear zones at fault terminations.

The change from brittle to ductile deformation styles around fault terminations as a function of distance from the Mono Creek Granite (Fig. 3) apparently is due to increased local temperatures during faulting. However, the actual material response about the fault terminations is a function of the local state of stress. To investigate this further, we compute the stress distribution around a fault in an elastic solid. Although the model assumes purely elastic behavior, first-order conclusions can be drawn for viscous and visco-elastic rheologies. The governing equations that relate stress to strain in elastic material are completely analogous to those relating stress and strain rate in visco-elastic and viscous substances (Johnson 1970, p. 272). In particular, solutions for stresses in plane strain of an elastic body are solutions for stresses in incompressible, viscous bodies with the same boundary conditions (Johnson 1970, p. 278). However, the development of large strains and anisotropic fabrics, and non-linear rheologies, clearly are not addressed in our models. Instead, we model the stress field caused by a few millimeters of displacement on the faults. Inelastic deformation continuously relaxes these stresses. Stress fields computed from models of equidimensional faults in three dimensions do not differ significantly from plane strain models except near the upper and lower fault peripheries (Bürgmann & Pollard 1992). Shortening in contractional fault steps results in vertical extension in non-plane strain models.

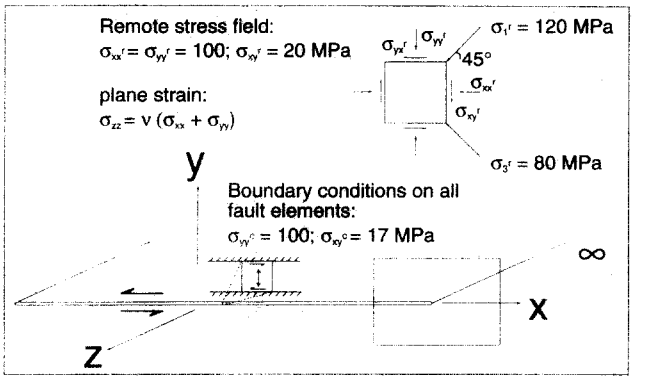


Fig. 12. Boundary conditions and model geometry of a fault surface in an elastic, isotropic and homogeneous material. Compressional stresses are positive and shear stresses are positive as shown. The fault is idealized to extend infinitely in the out-of-phase z-direction.

The stress field around a fault termination was determined using the boundary element method (Crouch & Starfield 1983) implemented as the program Frac2D by Thomas & Pollard (1993). The model assumes a homogeneous, isotropic, linear elastic solid under conditions of two-dimensional elastostatic plane strain. The vertical dimension of the fault is assumed to be much greater than its length and we postulate no vertical variations in geometry or boundary conditions.

A 20 m long left-lateral fault is divided into 80 displacement-discontinuity boundary elements, each 25 cm long. Compressive stress is taken to be positive. Mean remote stress ($\sigma_m^r = \sigma_{xx}^r = \sigma_{yy}^r = (\sigma_1^r + \sigma_3^r)/2$) is assumed to be 100 MPa based on the assumed depth of burial and a remote maximum shear stress ($\sigma_s^r = \sigma_{xy}^r = (\sigma_1^r - \sigma_3^r)/2$) of 20 MPa is applied. These input conditions constrain the remote maximum principal compressive stress ($\sigma_1^r = 120$ MPa) to be oriented 45° to the fault. This is approximately parallel to splay fractures along faults in the Lake Edison Granodiorite (within 30–60° of the fault trace). Fluid pressure, $P_p$, is assumed to be 70 MPa based on the distribution of dilatant fractures about fault steps that indicate fluid-pressure assisted fracture (Bürgmann & Pollard 1992).

The uniform strength of the fault elements was calculated using a Byerlee-type friction law that relates the shear stress on a fault ($\tau$) to the effective normal stress ($\sigma_n$), the coefficient of friction ($\mu$), and the inherent cohesion of the fault zone ($C$).

$$\tau = \sigma_n \mu + C. \quad (1)$$

With an effective fault-normal stress, $\sigma_n = \sigma_n^{lith} - P_p = 100$–$70$ MPa (Bürgmann & Pollard 1992), a coefficient of friction, $\mu = 0.4$, suggested for faults at hydrothermal conditions (Blanpied *et al.* 1992), and cohesion $C = 5$ MPa, we find the frictional strength $\tau$ of the fault to be 17 MPa. These values are only approximations of the conditions during faulting; they are constrained by observations of abundant veining indicating high fluid pressures and estimates of shear strength of the ductile-deforming fault gouge based on the orientation of secondary splay fractures and fabrics about fault steps that

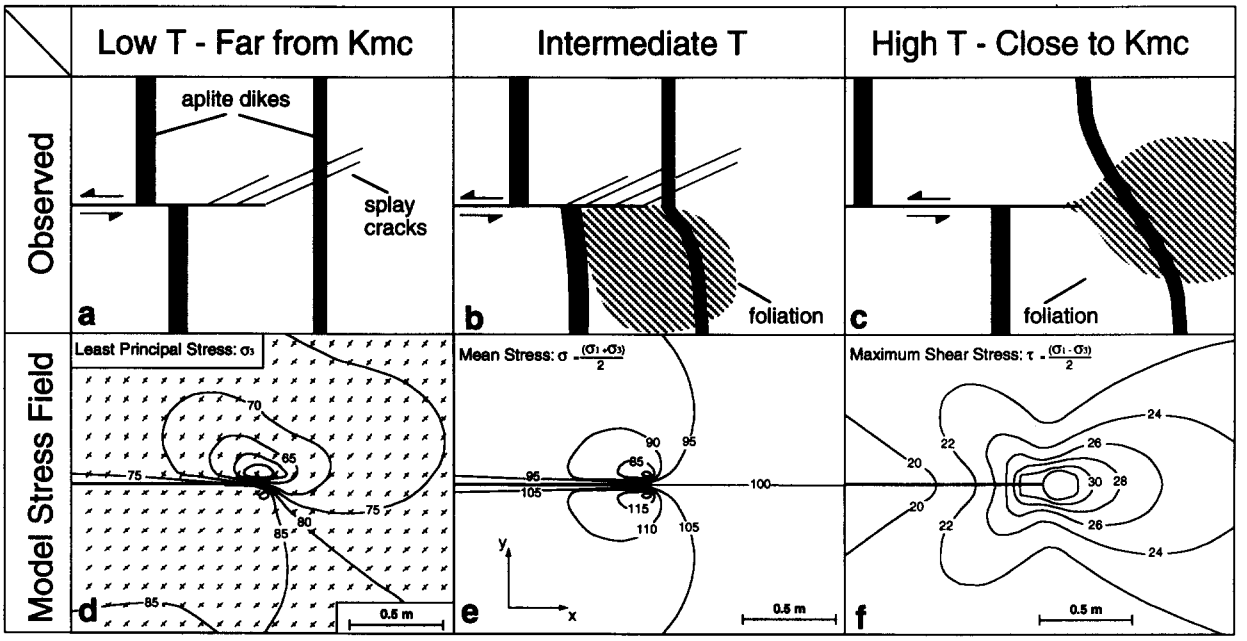


Fig. 13. (a)–(c) Schematic illustrations of fault-termination structures observed at various distances from the Mono Creek Granite (Fig. 3). (d)–(f) Components of the stress field that appear to control the deformation processes about the fault terminations.

indicate that faults had significant strength (Bürgmann & Pollard 1992).

Figures 13(a)–(c) show schematic illustrations of the three types of fault terminations found in the Lake Edison Granodiorite (Fig. 3). The lower panels in Figs. 13(d)–(f) show the magnitudes of key components of the stress field and the orientation of the principal stresses at one fault termination, all from the same model calculation. Least principal stress ($\sigma_3$, Fig. 13d) is at a minimum (least compressive) in the extensional quadrants (the NE and SW quadrants of the EW-trending, left-lateral fault) and is slightly increased from its remote magnitude (80 MPa) in the contractional quadrant. For splay fractures to form, the effective tensile stress, $\sigma_3(\text{eff}) = \sigma_3 - P_p$, must be larger than the tensile strength of the rock. It the fluid pressure is about 70 MPa, we would expect to find dilatant fractures parallel to the $\sigma_1$-direction near the fault termination in the extensional quadrant. The abundance of such splay fractures (Figs. 3a & b) and associated micro-cracking at fault terminations throughout the Bear Creek area is consistent with this assumption. Note that the splay fractures in Fig. 3(b) initiate at a higher angle and then propagate towards a lower angle, indicating a variable stress field due to stress perturbations near the fault termination.

The mean-stress component of the stress field (Fig. 13e) is anti-symmetrically distributed about the fault termination, and is increased by up to 20 MPa in the contractional quadrant and reduced by the same amount in the extensional quadrant. Ductile fabrics developed in the contractional quadrant of fault terminations, while splay fractures formed in the extensional quadrant at intermediate distances from the Mono Creek Granite (Fig. 3c). This is consistent with the pressure-weakening effect proposed by Bürgmann & Pollard (1992) that occurs under conditions close to the brittle–ductile transition. Apparently the side-by-side occurrence of brittle and ductile structures is caused by this difference in the mean stress component across the fault trace.

The maximum shear stress component of the stress field (Fig. 13f) shows a symmetrical distribution around the fault termination. Shear stress magnitudes are increased to 35 MPa immediately in front of the fault termination. Deformation laws involving viscous flow (e.g. by power-law creep) predict that high deformation rates correlate with high shear-stress magnitudes. In the Lake Edison Granodiorite high strains occur in a narrow region at the margin of the Mono Creek Granite where symmetric shear zones spread from the fault terminations (Fig. 3d). This indicates that temperatures in the immediate vicinity of the Mono Creek Granite were high enough to cause viscous deformation at fault terminations despite mean-stress differences.

## STRESS-DEPENDENT DEFORMATION ABOUT ECHELON FAULTS

Brittle and/or ductile structures about fault steps in the Lake Edison Granodiorite formed because of local stress perturbations. We evaluate elastic models of echelon fault steps to gain better understanding of the effects of the stress field on the structural development (Segall & Pollard 1980, Bürgmann & Pollard 1992). Secondary structures such as splay fractures may partially relax the stress perturbations. Even though permanent strains by viscous flow cannot be computed from elastic models, we find that flow laws that do not include an effect of mean stress on deformation rate do not predict the observed relationships.

The stress field associated with echelon fault steps is

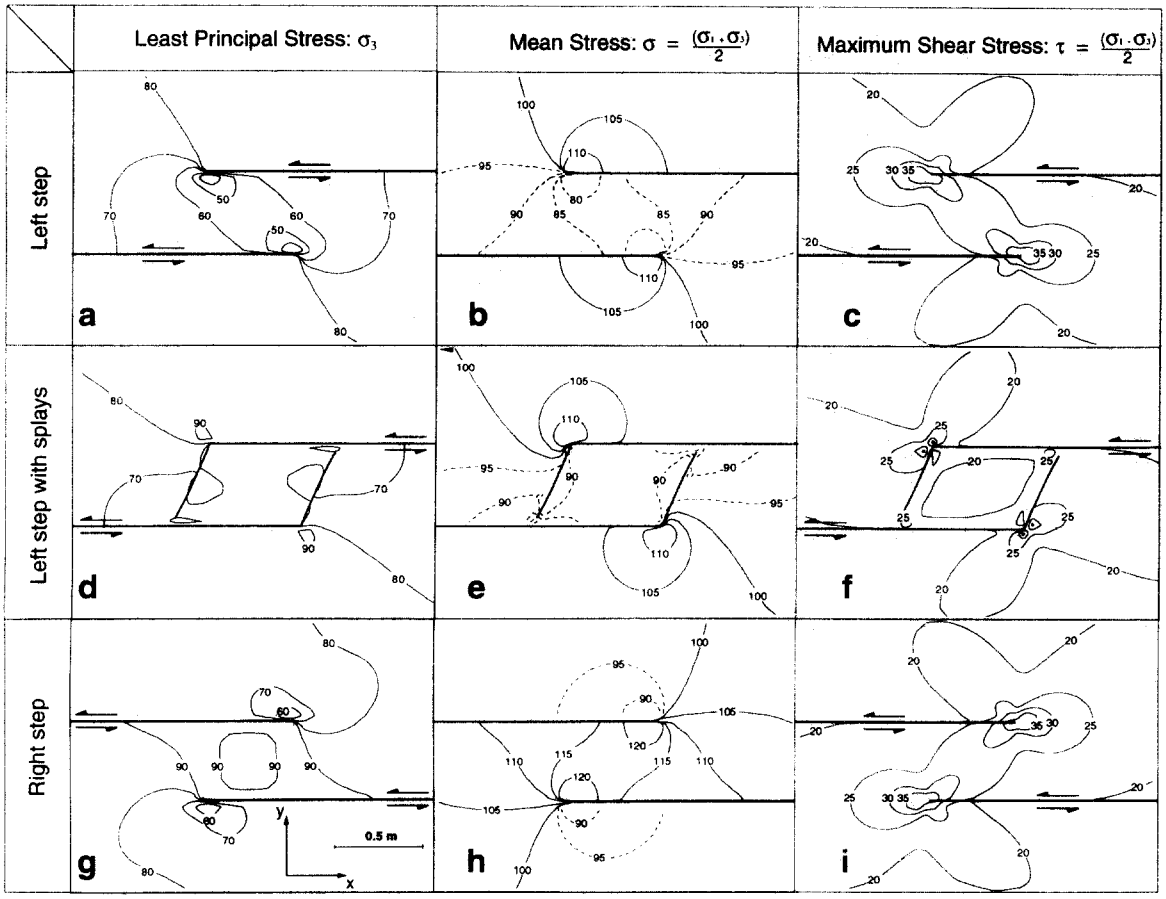


Fig. 14. Components of the stress field about two faults in left and right-stepping geometry. (a)–(c) Extensional left step, (d)–(f) left step with dilatant fractures growing within the fault step, (g)–(i) contractional step.

modeled using the boundary element method as described above. Two 10 m long left-lateral faults are arranged echelon with a left or right step of 45 cm width and 50 cm overlap. The amounts of separation and overlap of the echelon fault segments determine details of the perturbed stress field. However, the general conclusions drawn from the presented models apply to other geometries as well. Boundary conditions are the same as for the fault-termination models (Fig. 12). Figure 14 shows the stress fields associated with deformation about extensional left steps (Figs. 14a–c), left steps with splay fractures (Figs. 14d–f), and contractional right steps (Figs. 14g–i).

*Extensional steps*

Dilatant fractures form where the fluid pressure exceeds the applied least compressive stress, $\sigma_3$. Veins and fractures near fault terminations and fault discontinuities indicate that stress perturbations due to faulting may sufficiently reduce $\sigma_3$ to cause rock to break by dilatant fracture. The modeled stress fields associated with fault terminations and steps suggest that under the given boundary conditions such fractures form if $\sigma_3$ is less than ~70 MPa (Figs. 13d and 14a, d & g).

We investigate the effects of inelastic stress relaxation in an extensional step by allowing dilatant fractures to grow from the fault terminations of an extensional step (Figs. 14d–f). Fracture growth is introduced in our two-dimensional models with a fracture criterion at the crack tip (e.g. Hallam & Ashby 1990). The fractures are prescribed to grow by a 0.5 cm increment if the stress intensity factor, $K_I$, exceeds a critical stress intensity factor $K_{Ic} = 1.5$ MPa $m^{1/2}$ (Atkinson & Meredith 1987, p. 492). The newly formed elements are specified to have zero shear traction and normal tractions equivalent to the assumed fluid pressure of 70 MPa. The fractures propagate in a direction parallel to the local $\sigma_3$-orientation.

Figures 14(d)–(f) shows the stress fields and the fracture geometry about an extensional step with two splay fractures. The effective stresses within the step and the shear stress perturbations at the fault terminations are partly relaxed due to crack opening (Fig. 14d). Cracks in the fault step transfer slip between the two faults and reduce the stress perturbations at the fault discontinuity. The low magnitude of the mean and shear stress components in our models may explain the lack of extensive penetrative deformation near extensional steps in the Lake Edison Granodiorite.

*Contractional steps*

Bürgmann & Pollard (1992) suggest that a mean-stress dependent flow strength of granitic rock at brittle–ductile conditions is responsible for the observed

localization of mylonitic fabrics within the contractional stepovers in the Lake Edison Granodiorite. Whereas shear stress is increased within and around a contractional step (Fig. 14i), the mean stress is elevated only between the two step-bounding faults in our models (Fig. 14h). A possible mechanism of weakening may lie in the pressure dependence of hydrolytic weakening of quartz recognized in several experimental studies (e.g. Tullis & Yund 1980). Wall rock alterations and abundant veins and fluid inclusions in the Lake Edison Granodiorite indicate that faulting occurred in the presence of excess water.

We will evaluate existing constitutive flow laws for this pressure effect. Experimentally observed constitutive flow laws of the form

$$\dot{\varepsilon} = A \cdot (\sigma_1 - \sigma_3)^n \cdot e^{(\Delta H/RT)} \quad (2)$$

(e.g. Sibson 1983) predict that deformation rate (and thus fabric development) is a function of the differential stress and temperature. In equation (2) $\dot{\varepsilon}$ is the deformation rate, A is a material parameter, $n$ is the stress exponent, $\Delta H$ is a general activation energy term for creep, $T$ is the temperature in Kelvin, and $R$ is the universal gas constant. For example, flow-law parameters for wet Westerly Granite determined at constant confining pressure ($\sigma_2 = \sigma_3 = 1000$ MPa) are $n = 1.9$, A $= 10^{-3.7}$ MPa$^{-n}$s$^{-1}$, and $\Delta H = 137$ kJ mol$^{-1}$ (Hansen & Carter 1983). In this flow law, $\dot{\varepsilon}$ is independent of pressure, except for a weak pressure dependence of $\Delta H$. Equation (2) therefore predicts increased deformation rates and larger permanent strains in zones of increased maximum shear stress (e.g. Fig. 13f and 14c, f & i).

Weertman (1970) suggested a different flow law for creep by diffusion mechanisms,

$$\dot{\varepsilon} = B \cdot (\sigma_1 - \sigma_3)^m \cdot e^{[-g(T_m/T)]}, \quad (3)$$

where $B$ and $g$ are empirically derived constants, $m$ is the stress exponent, and $T_m$ is the melting temperature of the same rock at the current pressure. The effect of pressure, composition changes, and the chemical environment on the solidus temperature, $T_m$, can be used to quantify the effect of these parameters on creep (Borch & Green 1989). Borch & Green (1989) found in experiments that the effect of pressure on melting provides the scale for the effect of mean stress on dislocation creep of olivine. They found that changes in water content, which also change the solidus, have a corresponding effect on the flow stress. Normalization to the appropriate solidus may 'remove' the hydrolytic weakening effect (Borch & Green 1989).

We apply the diffusion creep law of Weertman (1970) to granitic rocks to examine the magnitude of the predicted pressure effect. Lacking enough deformation data to directly compute a mean-stress dependent flow law, we determine a law of the form given in equation (3) by setting the two flow laws (equations 2 and 3) equal at the experimental conditions. We use the solidus determined for samples of Sierran granodiorite (Mt. Givens Granodiorite) of similar composition to the Lake Edison Granodiorite in the presence of excess water (Piwinskii

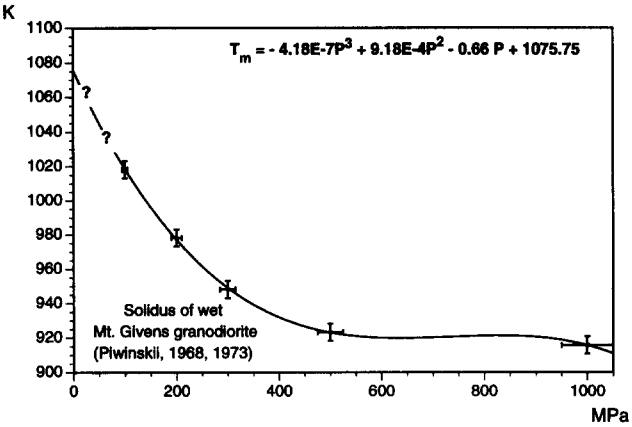


Fig. 15. Experimentally determined solidus for Mt. Givens Granodiorite with excess water from 100–1000 MPa (Piwinskii 1968, 1973).

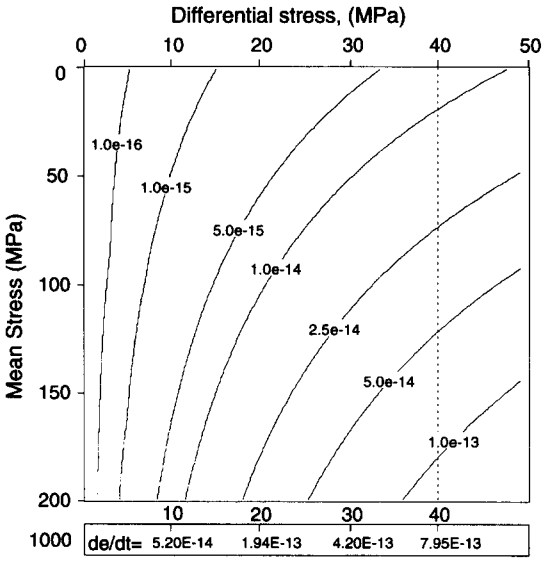


Fig. 16. Contour plot of deformation rates at 350°C as a function of pressure and differential stress calculated from equations (3) and (4). Flow law parameters for wet Westerly Granite at 1000 MPa are from Hansen & Carter (1983).

1968, 1973). A third-order polynomial is least-squares fit to the measured solidus temperature as a function of pressure (Fig. 15).

$$T_m(P) = -4.18\text{E-}7\,P^3 + 9.18\text{E-}4\,P^2 - 0.66\,P + 1075.75. \quad (4)$$

Assuming that the solidus of wet Westerly Granite is not significantly different from that of wet Mt. Givens Granodiorite we can set $B = A = 10^{-3.7}$ MPa$^{-n}$ s$^{-1}$, $m = n = 1.9$, and $g = \Delta H/(RT_m) = 137$ kJ mol$^{-1}$/(8.3144 J K$^{-1}$ mol$^{-1}$ $T_m$), where $T_m = 915$ K is the experimentally determined temperature of the solidus at 1000 MPa.

Using equation (3) we determine deformation rates in the presence of abundant water for the range of pressures and differential stress' at 350°C (Fig. 16). The pressure-dependent deformation rates extrapolated from equation (2) are shown below the contoured deformation rates calculated from equation (3). The flow law of form of equation (2) (Hansen & Carter 1983) predicts

higher deformation rates at lower pressures than those extrapolated from equation (3) because the solidus temperature at 1000 MPa (915 K) is significantly lower than at 100 MPa (1018 K). Figure 16 shows that the predicted pressure effect becomes more significant at lower pressures due to a larger gradient of the solidus at lower pressures (Fig. 15). The predicted pressure effect is less pronounced at higher temperatures. From equations (3) and (4) we find that an increase of pressure from 100 MPa to 120 MPa at a differential stress of 40 MPa (dashed line) causes an increase of deformation rates by ~30% at 350°C.

Temperatures of 300–350°C are thought to occur at depths of ~10–15 km in seismically active areas such as the San Andreas fault system (Lachenbruch & Sass 1980). An increase of pressure from 400 to 420 MPa (~15 km) at 350°C would be expected to result in an increase of deformation rate of only ~7%. We may therefore not expect the pressure-weakening effect we observe in the Lake Edison Granodiorite to play an important role where geothermal gradients are not significantly elevated. Constitutive models of inelastic rheologies and rock deformation experiments at a variety of pressures to test pressure-dependent flow laws are needed to better constrain the proposed relationships. The diffusion creep law of Weertman (1970) appears to be qualitatively consistent with the observed relationships of localized fabric development in the Lake Edison Granodiorite and model stress field.

## CONCLUSIONS

This research suggests that in the brittle–ductile deformation regime at a given temperature and in the presence of hydrothermal fluids the local state of stress can determine the locally active deformation mechanisms in granitic rock. Detailed field and microscopic observations show that brittle and ductile deformation features in the Lake Edison Granodiorite are localized near fault terminations and fault steps. Boundary element models of faults in an elastic body allow us to evaluate the stress inhomogeneities at fault terminations and in fault stepovers. We conclude the following about the effects of stress-field perturbations due to faulting on deformation textures and the acting deformation mechanisms in the Lake Edison Granodiorite:

(1) Stress concentrations due to fault slip determine the style and magnitude of strain accommodation in the wall rock.

(2) Tensile effective least principal stress favors strain accommodation by dilatant fracturing in the extensional quadrant at fault terminations and within extensional steps throughout most of the Lake Edison Granodiorite. These fractures formed active conduits for hydrothermal fluid flow.

(3) Increased mean stress within contractional steps and in the contractional quadrants of fault terminations leads to a ductile deformation style (crystal–plastic flow of quartz) at conditions close to the brittle–ductile transition. Geochemical analyses show that mass was transferred out of the contractional steps by viscous flow, not by diffusive mass transfer.

(4) At the localities investigated, only within about 100 m of the Mono Creek Granite do we find fewer fractures and well developed ductile fabrics at fault terminations that indicate ductile flow as a direct consequence of increased maximum shear stress at higher temperatures.

(5) Constitutive flow laws that do not include a pressure effect on deformation rate fail to predict the observed distribution of ductile fabrics.

*Acknowledgements*—This research was supported by the Geological Society of America, Sigma Xi, The McGee research fund of the Geology Department, and the Rock Fracture Project of Stanford University. Ramón Arrowsmith, Peter Christiansen, Steve Martel, Michael Pollard, and Betty Suh helped with the field work. Joel Sparks gave advice on the geochemical analyses. We thank Pamela Burnley for pointing out pressure-dependent flow laws. Elizabeth Miller, Mark Swanson, Jan Tullis, Associate Editor Steven Wojtal, and an anonymous reviewer provided very helpful comments and suggestions.

## REFERENCES

Ague, J. J. 1991. Evidence for major mass transfer and volume strain during regional metamorphism of pelites. *Geology* **19**, 855–858.

Atkinson, B. K. & Meredith, P. G. 1987. Experimental fracture mechanics data for rocks and minerals. In: *Fracture Mechanics of Rock* (edited by Atkinson, B. K.). Academic Press, London, 477–525.

Aydin, A. & Nur, A. 1982. Evolution of pull-apart basins and their scale independence. *Tectonics* **1**, 91–105.

Bateman, P. C. 1992. Plutonism in the central part of the Sierra Nevada Batholith, California. *Prof. Pap. U.S. geol. Surv.* **1483**, 1–186.

Best, M. G. 1982. *Igneous and Metamorphic Petrology*. W. H. Freeman and Co., San Francisco, California.

Bilham, R. & King, G. P. C. 1989. The morphology of strike-slip faults: Examples from the San Andreas fault, California. *J. geophys. Res.* **94**, 10204–10216.

Blanpied, M. L., Lockner, D. A. & Byerlee, J. D. 1992. An earthquake mechanism based on rapid sealing of faults. *Nature* **358**, 574–576.

Borch, R. S. & Green, H. W. 1989. Dependence of creep in olivine on the homologous temperature and its implications for flow in the mantle. *Nature* **330**, 345–348.

Brace, W. F. & Bombolakis, E. G. 1963. A note on brittle crack growth in compression. *J. geophys. Res.* **68**, 3709–3713.

Bürgmann, R. & Pollard, D. D. 1992. Influence of the state of stress on the brittle–ductile transition in granitic rock: evidence from fault steps in the Sierra Nevada, California. *Geology* **20**, 645–648.

Busby-Spera, C. J. & Saleeby, J. B. 1990. Intra-arc strike-slip fault exposed at batholithic levels in the southern Sierra Nevada, California. *Geology* **18**, 255–259.

Byerlee, J. D. 1968. Brittle–ductile transition in rocks. *J. geophys. Res.* **73**, 4741–4750.

Chinnery, M. A. 1965. The vertical displacement associated with transcurrent faulting. *J. geophys. Res.* **70**, 4627–4632.

Christiansen, P., Bürgmann, R. & Pollard, D. D. 1992. Relationship between faulting and hydrothermal circulation during cooling of granitoid plutons. *Geol. Soc. Am. Abstr. w. Prog.* **24**, 15.

Christie-Blick, N. & Biddle, K. T. 1985. Deformation and basin formation along strike-slip faults. In: *Strike-slip Deformation, Basin Formation and Sedimentation* (edited by Biddle, K. T. & Christie-Blick, N.). *Soc. econ. Paleont. Mineral. Spec. Pub.* **37**, 1–34.

Cox, S. J. D. & Scholz, C. H. 1988. On the formation and growth of faults: An experimental study. *J. Struct. Geol.* **10**, 413–430.

Crouch, S. L. & Starfield, A. M. 1983. *Boundary Element Methods In Solid Mechanics*. Unwin Hyman, London.

Crowell, J. C. 1974a. Origin of late Cenozoic basins in southern California. In: *Tectonics and Sedimentation* (edited by Dickinson, W. R.). *Soc. econ. Paleont. Mineral. Spec. Pub.* **22**, 190–204.

Crowell, J. C. 1974b. Sedimentation along the San Andreas fault, California. In: *Modern and Ancient Geosynclinal Sedimentation* (edited by Dott, R. H. & Shaver, R. H.). *Soc. econ. Paleont. Mineral. Spec. Pub.* **19**, 292–303.

Cruikshank, K. M., Zhao, G. & Johnson, A. M. 1991. Duplex structures connecting fault segments in Entrada Sandstone. *J. Struct. Geol.* **13**, 1185–1196.

Davies, R. K. & Pollard, D. D. 1986. Relations between left-lateral strike-slip faults and right-lateral monoclinal kink bands in granodiorite, Sierra Nevada, California. *Pure & Appl. Geophys.* **124**, 177–201.

Deng, Q., Wu, D., Zhang, P. & Chen, S. 1986. Structure and deformational character of strike-slip fault zones. *Pure & Appl. Geophys.* **124**, 203–224.

Dibblee, T. W., Jr. 1977. Strike-slip tectonics of the San Andreas fault and its role in Cenozoic basin evolvement. In: *Late Mesozoic and Cenozoic Sedimentation and Tectonics in California* (edited by Nilsen, T. H.). San Joaquin Geological Society Bakersfield, California, 26–38.

Fletcher, R. & Pollard, D. D. 1981. An anticrack mechanism for stylolites. *Geology* **9**, 419–424.

Gamond, J. F. 1987. Bridge structures as sense of displacement criteria in brittle fault zones. *J. Struct. Geol.* **9**, 609–620.

Gibson, R. G. 1990. Nucleation and growth of retrograde shear zones: an example from the Needle Mountains, Colorado, U.S.A. *J. Struct. Geol.* **12**, 339–350.

Granier, T. 1985. Origin, damping and pattern of development of faults in granite. *Tectonics* **4**, 721–737.

Hallam, S. D. & Ashby, M. F. 1990. compressive brittle fracture and the construction of multi-axial failure maps. In: *Deformation Processes in Minerals, Ceramics and Rocks* (edited by Barber, D. J. & Meredith, P. G.). The Mineralogical Society of Great Britain and Ireland, Unwin Hyman London, 84–108.

Hansen, F. D. & Carter, N. L. 1983. Semibrittle creep of dry and wet Westerly granite at 1000 MPa. *Proc. U.S. Symp. on Rock Mechanics* **24**, 429–447.

Harris, R. A. & Day, S. M. 1993. Dynamics of fault interaction: parallel strike-slip faults. *J. geophys. Res.* **98**, 4461–4472.

Hempton, M. R. & Neher, K. 1986. Experimental fracture, strain and subsidence patterns over en-echelon strike-slip faults. *J. Struct. Geol.* **8**, 597–605.

Jackson, M. D., Endo, E. T., Delaney, P. T., Arnadottir, T. & Rubin, A. M. 1992. Ground ruptures of the 1974 and 1983 Kaoiki earthquakes, Mauna Loa volcano, Hawaii. *J. geophys. Res.* **97**, 8775–8798.

Johnson, A. M. 1970. *Physical Processes in Geology*. Freeman, Cooper, San Francisco, California.

King, G. C. P. & Nabelek, J. 1985. Role of fault bends in the initiation and termination of earthquake rupture. *Science* **228**, 984–987.

Kronenberg, A. K., Segall, P. & Wolf, G. H. 1990. Hydrolytic weakening and penetrative deformation within a natural shear zone. In: *The Brittle–Ductile Transition in Rocks—The Heard Volume* (edited by Duba, A. G., Durham, W. B., Handin, J. W. & Wang, H. F.). *Am. Geophys. Un.Geophys. Monogr.* **56**, 21–36.

Lachenbruch, A. H. & Sass, J. H. 1980. Heat flow and energetics of the San Andreas fault zone. *J. geophys. Res.* **85**, 6185–6223.

Lawn, B. R. & Wilshaw, T. R. 1975. *Fracture of Brittle Solids*. Cambridge University Press, Cambridge.

Lin, P. & Logan, J. M. 1991. The interaction of two closely splaced cracks: A rock model study. *J. geophys. Res.* **96**, 21,667–21,675.

Lister, G. S. & Snoke, A. W. 1984. S–C mylonites. *J. Struct. Geol.* **6**, 617–638.

Lockwood, J. P. & Moore, J. G. 1979. Regional deformation of the Sierra Nevada, California, on conjugate microfault sets. *J. geophys. Res.* **84**, 6041–6049.

Martel, S. J., Bürgmann, R. & Pollard, D. D. 1990. Ductile deformation associated with brittle faulting in granitic rock, Sierra Nevada, California. *EOS Trans. Am. Geophys. Un.* **71**, 1558.

Martel, S. J. & Pollard, D. D. 1989. Mechanics of slip and fracture along small faults and simple strike-slip fault zones in granitic rock. *J. geophys. Res.* **94**, 9417–9428.

Martel, S. J., Pollard, D. D. & Segall, P. 1988. Development of simple strike-slip fault zones in granitic rock, Mount Abbot quadrangle, Sierra Nevada, California. *Bull. geol. Soc. Am.* **99**, 1451–1465.

Mayo, E. B. 1941. Deformation in the interval Mt. Lyell-Mt. Whitney, California. *Bull. geol. Soc. Am.* **52**, 1001–1084.

McGarr, A., Pollard, D. D., Gray, N. C. & Ortlepp, W. D. 1979. Observations and analysis of structures in exhumed mine-induced faults. *U.S. Geol. Surv. Open-file Rept.* 79–1239, 101–120.

Naylor, M. A., Mandl, G. & Sijpensteijn, C. H. K. 1986. Fault geometries in basement-induced wrench faulting under different initial stress states. *J. Struct. Geol.* **8**, 737–752.

Page, B. M. & Engebretson, D. C. 1984. Correlation between the geologic record and computed plate motions for central California. *Tectonics* **3**, 133–155.

Paterson, M. S. 1978. *Experimental Rock Deformation—The Brittle Field*. Springer Verlag, New York.

Piwinskii, A. J. 1968. Experimental studies of igneous rock series central Sierra Nevada batholith, California. *J. Geol.* **76**, 548–570.

Piwinskii, A. J. 1973. Experimental studies of igneous rock series, central Sierra Nevada batholith, California: Part II. *Neues Jahb. Mineral., Monatsh.* **5**, 193–215.

Pollard, D. D. & Segall, P. 1987. Theoretical displacements and stresses near fractures in rocks: with applications to faults, joints, veins, dikes, and solution surfaces. In: *Fracture Mechanics of Rock* (edited by Atkinson, B. K.). Academic Press Inc., London, 277–349.

Pollard, D. D., Segall, P. & Delaney, P. T. 1982. Formation and interpretation of dilatant echelon cracks. *Bull. geol. Soc. Am.* **93**, 1291–1303.

Rodgers, D. A. 1980. Analysis of pull-apart basin development produced by en-echelon strike-slip faults. In: *Sedimentation in Oblique-slip Mobile Zones* (edited by Ballance, P. F. & Reading, H. G.). *Int. Assoc. Sedimentol. Spec. Publ.* **4**, 27–41.

Ross, J. V. & Lewis, P. D. 1989. Brittle–ductile transition. Semibrittle behavior. *Tectonophysics* **167**, 75–79.

Rutter, E. H. 1986. On the nomenclature of model of failure transitions in rocks. *Tectonophysics* **122**, 381–387.

Scholz, C. H. 1988. The brittle–plastic transition and the depth of seismic faulting. *Geol. Rdsch.* **77**, 319–328.

Scholz, C. H. 1990. *The Mechanics of Earthquakes and Faulting*. Cambridge University Press, Cambridge.

Segall, P., McKee, E. H., Martel, S. J. & Turrin, B. D. 1990. Late Cretaceous age of fractures in the Sierra Nevada batholith, California. *Geology* **18**, 1248–1251.

Segall, P. & Pollard, D. D. 1980. Mechanics of discontinuous faults. *J. geophys. Res.* **85**, 4337–4350.

Segall, P. & Pollard, D. D. 1983a. Joint formation in granitic rock of the Sierra Nevada. *Bull. geol. Soc. Am.* **94**, 563–575.

Segall, P. & Pollard, D. D. 1983b. Nucleation and growth of strike-slip faults in granite. *J. geophys. Res.* **88**, 555–568.

Segall, P. & Simpson, C. 1986. Nucleation of ductile shear zones on dilatant fractures. *Geology* **14**, 56–59.

Sharp, R. V. & Clark, M. 1972. Geologic evidence of previous faulting near the 1968 rupture on the Coyote Creek fault. *Prof. Pap. U.S. geol. Surv.* **787**, 131–140.

Sibson, R. H. 1983. Continental fault structure and the shallow earthquake source. *J. geol. Soc. London* **140**, 741–767.

Sibson, R. H. 1984. Roughness at the base of the seismogenic zone: Contributing factors. *J. geophys. Res.* **89**, 5791–5800.

Sibson, R. H. 1985. Stopping of earthquake ruptures at dilational steps. *Nature* **316**, 248–251.

Sibson, R. H. 1986a. Earthquakes and rock deformation in crustal fault zones. *Ann. Rev. Earth Planet. Sci.* **14**, 149–175.

Sibson, R. H. 1986b. Rupture interaction with fault jogs. In: *Earthquake Source Mechanics* (edited by Das, S., Boatwright, J. & Scholz, C.). *Am. Geophys. Un.Geophys. Monogr.* **37**, 157–168.

Sibson, R. H. 1987. Earthquake rupturing as a mineralizing agent in hydrothermal systems. *Geology* **15**, 701–704.

Simpson, C. 1985. Deformation of granitic rock across the brittle–ductile transition. *J. Struct. Geol.* **7**, 503–511.

Smith, R. B. & Bruhn, R. L. 1984. Intraplate extensional tectonics of the eastern basin-range: inferences on structural style from seismic reflection data, regional tectonics, and thermal-mechanical models of brittle–ductile deformation. *J. geophys. Res.* **89**, 5733–5762.

Stern, T. W., Bateman, P. C., Morgan, B. A., Newall, M. F. & Peck, D. L. 1981. Isotopic U–Pb ages of zircon from the granitoids of the central Sierra Nevada, California. *Prof. Pap. U.S. geol. Surv.* **1185**, 1–17.

Swanson, M. T. 1988. Pseudotachylyte-bearing strike-slip duplex structures in the Fort Foster Brittle Zone of southern Maine. *J. Struct. Geol.* **10**, 813–828.

Swanson, M. T. 1992. Fault structure, wear mechanisms and rupture processes in pseudotachylyte generation. *Tectonophysics* **204**, 223–242.

Tapponnier, P. & Brace, W. F. 1976. Development of stress-induced microcracks in Westerly granite. *Int. J. Rock Mech. Mining Sci.* **13**, 103–112.

Thomas, A. L. & Pollard, D. D. 1993. The geometry of echelon fractures in rock: implications from laboratory and numerical experiments. *J. Struct. Geol.* **15**, 323–334.

Tikoff, B. & Teyssier, C. 1992. Crustal-scale, en-echelon "P-shear" tensional bridges; a possible solution to the batholithic room problem. *Geology* **20**, 927–930.

Tschalenko, J. S. 1970. Similarities between shear zones of different magnitudes. *Bull. geol. Soc. Am.* **81**, 1625–1640.

Tullis, J. A. 1990. Experimental studies of deformation mechanisms and microstructures in quartzo-feldspathic rocks. In: *Deformation Processes in Minerals, Ceramics and Rocks* (edited by Barber, D. J. & Meredith, P. G.). The Mineralogical Society of Great Britain and Ireland, Unwin Hyman, London, 190–226.

Tullis, J. A. & Yund, R. A. 1977. Experimental deformation of dry Westerly granite. *J. geophys. Res.* **82**, 5705–5718.

Tullis, J. A. & Yund, R. A. 1980. Hydrolytic weakening of experimentally deformed Westerly granite and Hale albite rock. *J. Struct. Geol.* **2**, 439–451.

Tullis, J. A. & Yund, R. A. 1987. Transition from cataclastic flow to dislocation creep of feldspar: mechanisms and microstructures. *Geology* **15**, 606–609.

Tullis, J. A. & Yund, R. A. 1989. Hydrolytic weakening of quartz aggregates: the effects of water and pressure on recovery. *Geophys. Res. Lett.* **16**, 1343–1346.

Weertman, J. 1970. The creep strength of the earth's mantle. *Rev. geophys. Space Physics* **8**, 145–168.

Wong, T. F. 1982. Micromechanics of faulting in Westerly granite. **19**, 49–64.

Woodcock, N. H. & Fischer, M. 1986. Strike-slip duplexes. *J. Struct. Geol.* **8**, 725–735.